This is a peer-reviewed, accepted author manuscript of the following research article:
Basoglu, M. F., Kefal, A., Zerin, Z., & Oterkus, E. (2022). Peridynamic modeling of toughening enhancement in unidirectional fiber-reinforced composites with micro-cracks. Composite Structures, 297, [115950]. https://doi.org/10.1016/j.compstruct.2022.115950

PERIDYNAMIC MODELING OF TOUGHENING ENHANCEMENT IN UNIDIRECTIONAL FIBER-REINFORCED COMPOSITES WITH MICRO-CRACKS

Muhammed Fatih Basoglu[1], Adnan Kefal[2,3,4,*], Zihni Zerin[1], Erkan Oterkus[5]

[1] *Department of Civil Engineering, Ondokuz Mayis University, Samsun 55139, Turkey*

[2] *Faculty of Engineering and Natural Sciences, Sabanci University, Tuzla, Istanbul 34956, Turkey*

[3] *Integrated Manufacturing Technologies Research and Application Center, Sabanci University, Tuzla, Istanbul 34956, Turkey*

[4] *Composite Technologies Center of Excellence, Istanbul Technology Development Zone, Sabanci University-Kordsa, Pendik, Istanbul 34906, Turkey*

[5] *Department of Naval Architecture, Ocean and Marine Engineering, University of Strathclyde, Glasgow G4 0LZ, United Kingdom*

**Correspondence: adnankefal@sabanciuniv.edu*

Abstract: The matrix component of composite structures is generally brittle. In any damage occurrence, fracture propagates rapidly through the structure. This study proposes a novel toughening enhancement model for unidirectional (UD) composites to overcome these damage-propagation issues. The toughening mechanism is established by introducing the so-called micro defects/cracks for increasing the toughness of the matrix constituent of the composite structure. Mechanical simulations are performed utilizing a non-local continuum formulation known as Peridynamics (PD). The PD formulation facilitates modeling material discontinuities such as complex crack/defect formations with an arbitrary size, orientation, and location features in composite structures. Here, the toughening enhancement models are established by allocating various micro-crack formations in three different fiber orientations (0°, 45°, 90°) of UD composite plates. The toughening effects of micro-crack clusters are thoroughly analyzed by making comprehensive comparisons on the propagation speed of an initially introduced macro-crack and its tip strain energy density. As a result, various micro-crack distributions are established to provide an augmented toughness to the brittle composite materials, and their key features are assessed in detail.

Keywords: Peridynamics, Toughening, Composite, Fracture, Micro-Crack, Unidirectional Lamina.

1. Introduction

Composite structures serve as primary structural components in today's engineering applications because of their superior tensile stiffness and rigidity as well as low weight to stiffness ratios. However, the brittle nature of its matrix constituent makes composite structures prone to any damage occurrence, thereby leading to rapid fracture propagation through the structure. This can cause the entire fiber-matrix system to be completely dysfunctional under operational conditions. Albeit traditionally being overdesigned to circumvent any unexpected failure mechanisms, once a minor failure/defect initiates in the material, complex damage propagation in these structures may be unavoidable. In addition, one of the most critical and undesirable situations of engineering is the occurrence of risky cracks. Such an unexpected failure in a crucial structural component can cause catastrophic failure of the entire system, and thus the structure is rendered useless. Therefore, even if a crack initiates, the goal should be to preserve the material's high stiffness by increasing the time for the damage to propagate in the degraded structural components.

A solution can be sought for this problem by increasing the toughness of brittle materials. For instance, small structural features such as micro-defects with random orientation/allocation can increase the toughness of brittle structures [1-4]. In fact, in the last few decades, tailored distribution of micro-cracks has been extensively studied to introduce practical toughening mechanisms for brittle materials. Depending on the shape, size, density, and location, these defects substantially affect the propagation of the macro-crack in the structure [5-8]. Various research studies were dedicated to addressing this issue in isotropic materials [5, 9, 10]. However, this critical application, i.e., toughening enhancement, is limited for composite structures in literature. Therefore, it is necessary to adopt a similar strategy for examining the effects of micro-defects on the structural response of laminated composite materials.

Moreover, the interaction between macro crack and micro defects has been investigated experimentally in literature [11-14]. Although experimental tests are quite important, numerical tools are potentially preferable to simulate fracture mechanics of structures due to their low cost and inconvenience of the experiments. Several analytical studies investigated the interaction of single or multiple micro-cracks with macro-cracks [3, 8, 15]. To solve complex crack interaction problems, assumptions are made in approaches based on classical continuum mechanics (CCM) to simplify the problem. For example, while the interactions between main-cracks and micro-cracks are investigated in analytical calculations, the interactions between micro-cracks are frequently neglected [16, 17]. This should not be the case for understanding

the toughening mechanism of micro-cracks, as their interaction is always dominated under complex loading conditions. Hence a need is evident for simulating the propagation of micro-damages based on a robust computational algorithm.

In analytical approaches, micro defects are defined by decreasing the elastic constant while creating homogenized models [18, 19]. As numerical approaches, various finite element method (FEM) versions such as element-erosion, cohesive-zone, and extended-FEM (X-FEM) are used in crack propagation modeling. In the element-erosion and the cohesive-zone methods, accurate results may not always be feasible due to the inherent assumptions of the methods. For instance, the crack propagation path is dependent on the element mesh-size [20]. On the other hand, this deficiency has been eliminated in the X-FEM method, and the crack propagation was modeled more accurately [21-26]. However, X-FEM has some shortcomings in predicting crack nucleation/initiation and requires the usage of level-set methods and other extra criteria to simulate accurate crack branching [27]. Hence, a more consistent approach is needed to predict crack nucleation, propagation, and interactions.

With the introduction of Peridynamics (PD), the shortcomings of CCM-based methods mentioned above have been completely eliminated by leveraging the superior features of the theory [28, 29]. Essentially, PD is a non-local theory that uses integrodifferential equations to solve the equation of motion of a continuum. Thus, its mathematical formulation is valid regardless of any structural discontinuity. Besides, except for its assumptions, no additional concept is needed to perform fracture mechanics simulations based on PD. Hence, it enables modeling of complex crack interactions, which can be introduced in the structure with an arbitrary size and orientation at different positions. The initial form of the PD, the *so-called* bond-based theory, has been successfully implemented for tackling problems including crack nucleation, propagation, and interaction [30-35]. With state-based PD formulation [36], the restrictions of the bond-based theory were removed such that the formulation becomes applicable for broader class of materials having different Poisson effect.

Apart from those major improvements of the PD theory mentioned above, various other research studies have proven the capability of PD for structural/fracture mechanics of materials and structures. For example, the convergence of PD to classical elasticity theory was investigated [37]. Moreover, in fiber-reinforced composites, crack propagation predictions of PD under mechanical and thermal loading were demonstrated [38]. In an experimental study [39], the damage propagation estimates of fiber-reinforced composites were validated by utilizing non-ordinary state-based PD. Furthermore, experimental tests were conducted to

validate capability of ordinary state-based PD for modeling crack coalescences in composites [40]. Additionally, dynamic fracture analyses were carried out in a polycrystalline microstructure by a proposed bond-based PD model [41]. Besides, fracture mechanics simulations of functionally graded materials (FGMs) were performed using ordinary state-based PD [42, 43]. In particular, toughness enhancement strategies were also proposed for FGMs [43]. For damage prediction of complex structures, a combined PD and finite element analyses approach was used [44, 45]. In addition, various other multi-physics and multi-scale problems were solved based on PD theory [46, 47]. Likewise, PD thermo-mechanics and heat conduction equations were derived and applied to various problems [48, 49]. The plasticity issue was studied within the framework of PD theory [50]. The comprehensive explanation of the theory and a detailed literature review can be found in [51, 52]. Most recently, PD theory has been coupled with optimization algorithms for finding the best material deposition on a given structural domain that may include discontinuity [53]. This approach was also utilized for multi-material [54] and continuous density-based [55] topology optimization of cracked structures.

Up until now, toughening effects of micro-defects and stop-holes on brittle fracture were investigated only for isotropic materials [34, 35, 56, 57]. Nevertheless, to the best of the authors' knowledge, there is no research study dedicated to micro-crack toughening enhancement of composite materials using neither CCM nor PD. Essentially, such an important problem must be addressed to be able to substitute mechanically toughened structures for pristine material to avoid catastrophic crack propagation in lamina composites. The main and novel aim of this study to fill this gap in the literature by making an extensive investigation of micro-crack allocations to tailor toughness properties of lamina composites. To perform mechanical analysis of structures effectively and accurately with micro-cracks, Peridynamics theory is adopted to develop an efficient toughening computational model. After verifying the PD implementation with numerical/experimental results available in the literature, the effect of various micro-crack clusters on the toughness of UD composite laminae is studied for three different fiber orientations (0°, 45°, 90°). In the evaluations, main-crack tip strain energy density and propagation speed parameters are taken into consideration for developing various toughness enhancement strategies for composite structures.

The rest of the study is structured as follows. In next section, mathematical description of bond-based PD theory for composite laminae is given. In section 3, a numerical and an experimental benchmark studies reported in [38] and [39] are revisited. In first benchmark [38],

the analytical deformation results of the undamaged lamina under tensile load are validated with bond-based PD composite code results. In next benchmark [39], the cases of fiber-reinforced composites with a central hole have been analyzed with PD composite code, and the damage prediction accuracy is validated. Later, numerical toughening models are introduced by employing micro-cracks for composite laminae with various fiber orientations. Finally, concluding remarks related to toughening mechanisms studied herein are given in section 5.

2. Peridynamic Theory for Unidirectional Composites

In the traditional CCM approach used for the analysis of solid structures, the interaction of infinitely small constitutive material points of the body occurs by the action and reaction principle with adjacent material points (see Fig. 1). The equation of motion of the material point, $\boldsymbol{x}$, by using the conservation of linear momentum is therefore expressed as:

$$\rho(\boldsymbol{x})\,\ddot{\boldsymbol{u}}(\boldsymbol{x},t) = \nabla\cdot\boldsymbol{\sigma} + \boldsymbol{b}(\boldsymbol{x},t) \tag{1}$$

where the expressions $\rho(\boldsymbol{x})$, $\boldsymbol{b}(\boldsymbol{x},t)$ and $\ddot{\boldsymbol{u}}(\boldsymbol{x},t)$ represent the density, body force and acceleration of the material point at $\boldsymbol{x}$, respectively. The spatial derivatives in the divergence of stress tensor $\nabla\cdot\boldsymbol{\sigma}$ are undefined for any discontinuity in the structure, thereby making equation (1) invalid for modeling cracks.

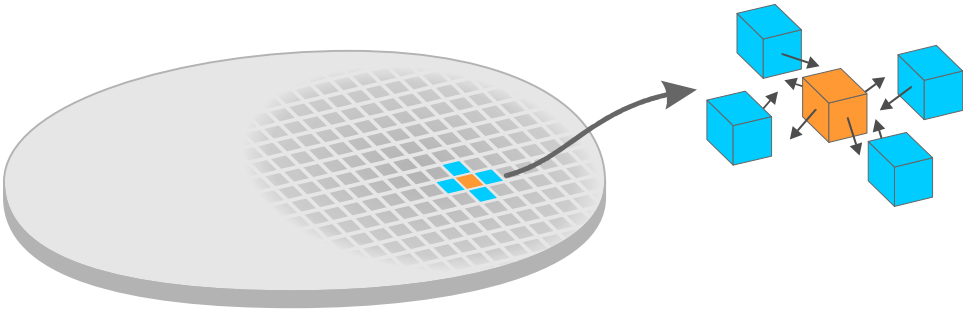

Fig. 1 Local interactions of Classical Continuum Mechanics

In Peridynamic theory, the divergence term in equation (1) was replaced with an integral expression by Silling [29] in 2000 as:

$$\rho(\boldsymbol{x})\,\ddot{\boldsymbol{u}}(\boldsymbol{x},t) = \int_{H} \boldsymbol{t}(\boldsymbol{\xi},\boldsymbol{\eta},t)\,dH + \boldsymbol{b}(\boldsymbol{x},t) \tag{2}$$

where the interaction force between the material points $\boldsymbol{x}$ and $\boldsymbol{x}'$, is expressed by $\boldsymbol{t}$, referred to as peridynamic force (Fig. 2). The most significant feature of PD is that derived equations do not contain any spatial derivatives. In other words, the forces between material points are

expressed by integration. Thus, this new form of the equation of motion allows the application of solid body mechanics in special cases such as discontinuity (crack) formation in the structure.

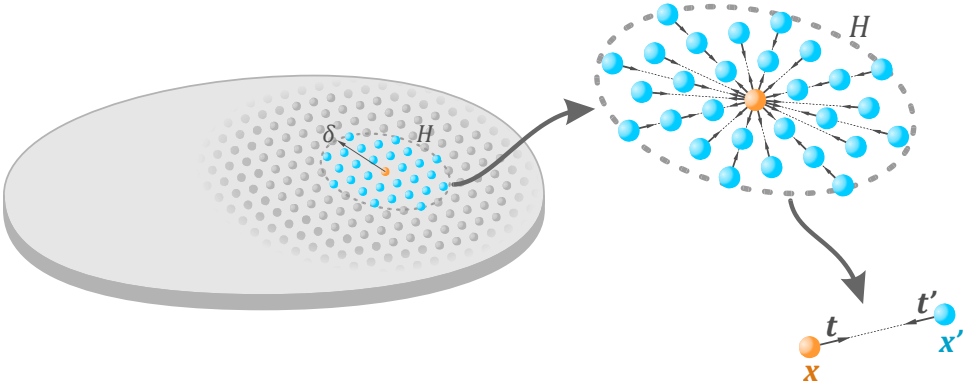

Fig. 2 Peridynamic horizon and non-local interaction forces

The integration given in equation (2) should be calculated over the H region, which contains all the material points interacting with given $\boldsymbol{x}$ point as depicted in Fig. 2. This region is referred to as peridynamic horizon or non-local interaction region (see Fig. 2). The peridynamic force, $\boldsymbol{t}$, is a function of the relative position vector before deformation, $\boldsymbol{\xi} = \boldsymbol{x}' - \boldsymbol{x}$, the relative displacement vector after deformation, $\boldsymbol{\eta} = \boldsymbol{u}' - \boldsymbol{u}$, and time, t. The direction of this force is aligned with the same direction as the relative position of the material points in the deformed configuration, namely along $\boldsymbol{\xi} + \boldsymbol{\eta} = (\boldsymbol{x}' + \boldsymbol{u}') - (\boldsymbol{x} + \boldsymbol{u})$ direction. According to bond-based formulation this force can be defined as:

$$\boldsymbol{t}(\boldsymbol{\xi}, \boldsymbol{\eta}, t) = f \frac{\boldsymbol{\xi} + \boldsymbol{\eta}}{|\boldsymbol{\xi} + \boldsymbol{\eta}|} \tag{3}$$

where f represents the peridynamic force magnitude, which can be defined for an elastic isotropic material as:

$$f = c\, s \tag{4}$$

where c and s denote the peridynamic material parameter and the stretch between material points ($\boldsymbol{x}$ and $\boldsymbol{x}'$), respectively. Here, the stretch can be defined as:

$$s = \frac{|\boldsymbol{\xi} + \boldsymbol{\eta}| - |\boldsymbol{\xi}|}{|\boldsymbol{\xi}|} \tag{5}$$

The material parameter c given in (4) can be analytically calculated by equating the strain energy densities of CCM and PD for a uniform tension loading condition. For two-dimensional (2-D, plane-stress state) and three-dimensional (3-D) conditions, the c parameter can be expressed for isotropic materials as [51]:

$$c = \frac{9E}{\pi h \delta^3} \quad \text{(for 2-D)} \tag{6}$$

$$c = \frac{12E}{\pi \delta^4} \quad \text{(for 3-D)} \tag{7}$$

where E represents the elastic modulus of the material and δ is the radius of the circular or spherical peridynamic horizon (non-local interaction region).

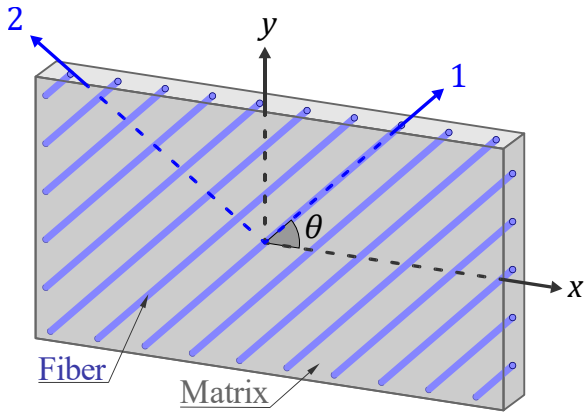

Fig. 3 Composite lamina with θ degree fiber orientation

Contrary to isotropic materials, it is necessary to define the directional dependency of material properties while modeling a UD composite lamina by peridynamics. To this end, two different material parameters are required to model a UD composite lamina in which the fibers are oriented in θ degree relative to the $\boldsymbol{x}$-axis, as illustrated in Fig. 3.

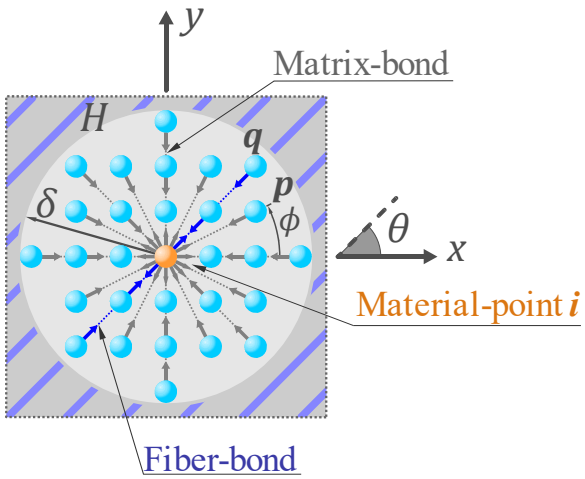

Fig. 4 Fiber and matrix bonds in the horizon of material point i

In Fig. 4, the interactions between i material point and all q material points in the fiber direction are defined as fiber bonds. Besides, the interactions between i material point and all p material points in all directions (including the fiber and matrix directions) are expressed as arbitrary bonds (see Fig. 4). The angle ϕ represents the direction of the bond between material

points (see Fig. 4). Material parameters for fiber and arbitrary bonds are expressed as c_f and c_m, respectively. Accordingly, the c parameter for a two-dimensional lamina in plane stress condition is expressed by Oterkus and Madenci [38] as:

$$c(\phi) = \begin{cases} c_f + c_m & \phi = \theta \\ c_m & \phi \neq \theta \end{cases} \tag{8}$$

where the angles ϕ and θ indicate the peridynamic bond angle and the fiber angle, respectively.

The fiber and arbitrary bond constants are derived by equating strain energy densities of CCM and PD for various loading conditions of the lamina, which can be expressed in terms of homogenized orthotropic material properties of the composite as:

$$c_f = \frac{2E_1(E_1 - E_2)}{\left(E_1 - \frac{1}{9}E_2\right)\frac{\pi h \delta^2}{n}\sum_{i=1}^{q}\xi_i} \tag{9}$$

$$c_m = \frac{8E_1E_2}{\left(E_1 - \frac{1}{9}E_2\right)\pi h \delta^3} \tag{10}$$

where E_i $(i = 1, 2)$ indicates the elastic constants of the composite material in the fiber and transverse directions. In (9) and (10), the ξ_i term is the distance between material point i and the material points interacting in the direction of the fiber in its horizon, and q represents the total number of these interactions. Also, n is the total number of material points within the horizon. To give an example, if the fiber direction is $\theta = 0$, $\sum_{i=1}^{q}\xi_i$ is calculated as 4δ and the number of material points in the horizon is $n = 29$. As a result, for a UD composite lamina with an angle $\theta = 0$, the parameter c_f can be expressed as:

$$c_f = \frac{2E_1(E_1 - E_2)}{\left(E_1 - \frac{1}{9}E_2\right)\frac{4\pi h \delta^3}{29}} \tag{11}$$

The following peridynamic strain energy density expression used in deriving the material parameter for any x material point:

$$U_{PD} = \frac{1}{2}\int_H w\, dH \tag{12}$$

where w micro potential is defined as:

$$w = \frac{1}{2} f\, s\, |\boldsymbol{\xi}| \tag{13}$$

To model damage in the composite lamina, the following concept is adopted. If the bond stretch between two material points exceeds the critical value, such as s_0, it is assumed that the bond between these two material points is broken, and their interaction is not concerned anymore. This is an elastic material behavior model without any permanent deformation.

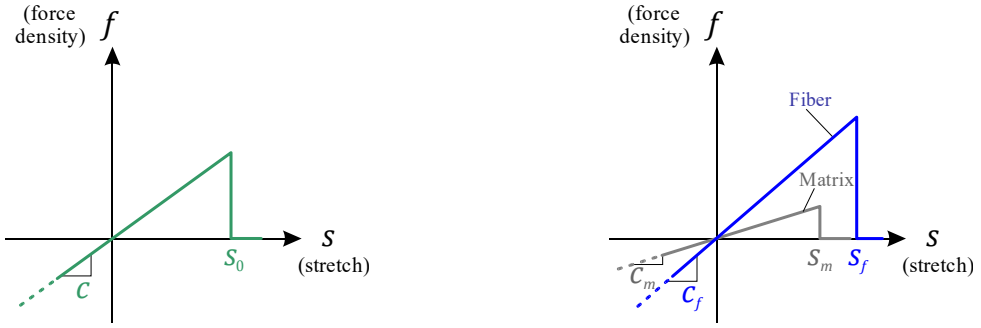

(a) (b)

Fig. 5 Elastic behavior models and damage criteria of isotropic (a) and composite materials (b)

As shown in Fig. 5, there is only one damage criterion in an isotropic material, while damage criteria are defined separately for fiber and arbitrary bonds in composite material. By multiplying a failure parameter $\mu(\boldsymbol{\xi}, t)$ with the peridynamic force expression given in (3), the variation of the interaction between material points due to damage can be considered as:

$$\boldsymbol{t} = \mu(\boldsymbol{\xi}, t)\, f \frac{\boldsymbol{\xi} + \boldsymbol{\eta}}{|\boldsymbol{\xi} + \boldsymbol{\eta}|} \tag{14}$$

Here, the failure parameter is defined as:

$$\mu(\boldsymbol{\xi}, t) = \begin{cases} 1 & \text{if } s(\boldsymbol{\xi}, t') < s_0 \;\;,\;\; (0 < t' < t) \\ 0 & \text{otherwise} \end{cases} \tag{15}$$

where s_0 is the critical stretch value. Moreover, the failure parameter given in (15) can be expressed as follows for a composite material model:

$$\mu(\boldsymbol{\xi}, \phi, t) = \begin{cases} 1 & \text{if } \phi = \theta \text{ and } s(\boldsymbol{\xi}, t') < s_f \;\;,\;\; (0 < t' < t) \\ 1 & \text{if } \phi \neq \theta \text{ and } s(\boldsymbol{\xi}, t') < s_m \;\;,\;\; (0 < t' < t) \\ 0 & \text{otherwise} \end{cases} \tag{16}$$

where s_f, s_m indicate the critical tensile stretches of fiber and matrix bonds, respectively. Detailed explanations for determining these parameters are available in Oterkus et al. [44]. Also, the weighted ratio of the number of broken bonds to the total number of bonds within the

horizon, H, of a material point is the local damage of the material point and expressed as follows:

$$\varphi(\boldsymbol{x}, t) = 1 - \frac{\int_H \mu(\boldsymbol{\xi}, t) dH}{\int_H dH} \tag{17}$$

Therefore, the grade of damage is defined on a closed interval as [0,1], where 0 means no damage at all and 1 means complete damaged material point. Moreover, damage values equal to or greater than 0.5 means cracking has occurred.

In numerical analysis, the peridynamic equation of motion given in (2) can be utilized in the form below:

$$\rho(\boldsymbol{x}_i)\, \ddot{\boldsymbol{u}}(\boldsymbol{x}_i, t) = \sum_{j=1}^{n} \boldsymbol{t}\big(\boldsymbol{x}_j - \boldsymbol{x}_i, \boldsymbol{u}_j - \boldsymbol{u}_i, t\big) V_j + \boldsymbol{b}(\boldsymbol{x}_i, t) \tag{18}$$

where n is the number of j material points within the horizon of material point i. Also, V_j represents the volume of each j material point.

3. Benchmark Analysis

In this section, results of benchmark test cases are presented to validate the proposed peridynamic model for composite structures. First, PD deformation results of a lamina under tensile load are compared with the analytical displacement solution obtained in [38]. Since this comparison validates our PD implementation for a lamina without any initial damage, the crack propagation accuracy of the PD composite model is examined in the second test case. Namely, for a UD lamina subjected to tensile loading, the experimental crack propagation patterns [39] are used to validate the damage predictions of the PD analysis.

3.1. Validation by Analytical Solutions

For the validation case, the undamaged lamina problem with 0° fiber orientation under tensile load considered in [38] is revisited (see Fig. 6). The lamina's length, width, and thickness are specified as 152.4 mm, 76.2 mm, and 0.1651 mm, respectively. The elastic moduli of the lamina are E_1=159.96 GPa and E_2=8.96 GPa in fiber and transverse directions, respectively, and the Poisson's ratio is v=1/3. The peridynamic model discretization is created by using a single material-point layer with a grid size of Δx=0.635 mm and the size of the horizon is specified as $\delta = 3.015\ \Delta x$. To compare with analytical solutions based on classical continuum mechanics, crack initiation is not allowed in the analysis.

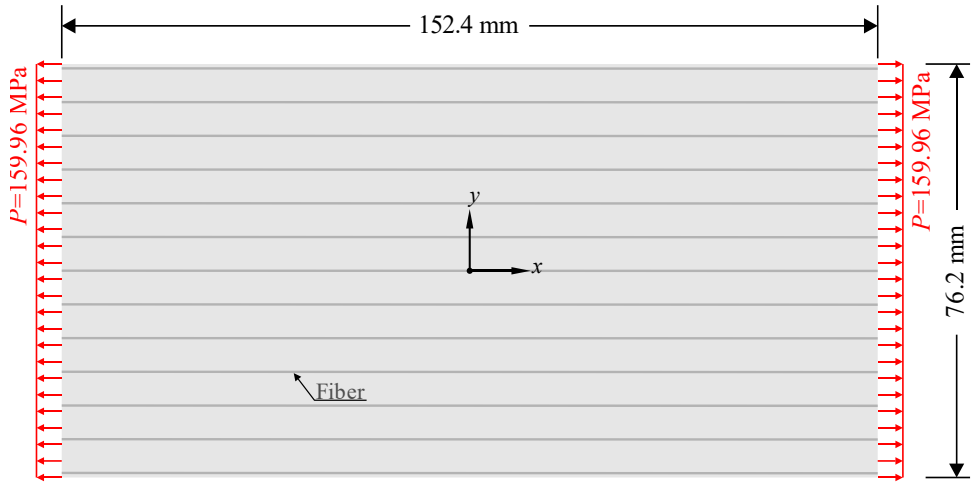

Fig. 6 *Analysis setup of the undamaged lamina problem with 0° fiber orientation under tensile load considered in Oterkus and Madenci [38].*

The lamina is subjected to a tensile load of P=159.96 MPa at its left and right edges. The variation of horizontal and vertical displacement components along x and y directions, respectively, are compared with the analytical results as shown in Fig. 7. Analytical results based on classical continuum mechanics are computed as: $u_x = \frac{P}{E_1}x$, $u_y = -\nu_{12}\frac{P}{E_1}y$. According to the displacement variations presented in Fig. 7, there is a clear agreement between analytical and peridynamic results for both displacement components, thereby validating the superior accuracy of present PD composite model as well as our computational implementation.

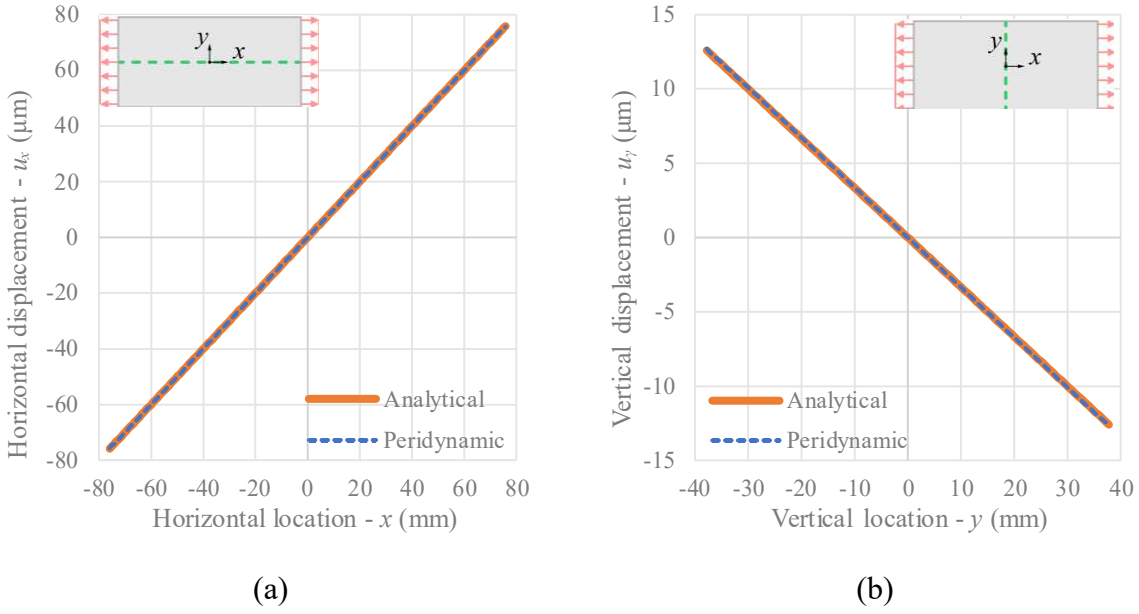

Fig. 7 *(a) Horizontal displacements along the central x axis, and (b) Vertical displacements along the central y axis.*

3.2. Validation by Experimental Results

In this section, peridynamic analysis of unidirectional lamina rupture experiments with a hole in the middle considered in the study of Shang et al. [39] is performed. In the experiments, specimens with a length of L = 100 mm, a width of W = 50 mm, a thickness of t = 1.0 mm and a hole diameter of D = 10 mm are considered with three different fiber orientations of 0°, 45°, and 90° [39] (see Fig. 8). The elastic moduli of T300 carbon fiber/epoxy composite lamina specimens are E_1=133.0 GPa and E_2=8.0 GPa in fiber and transverse directions, respectively, and Poisson's ratio is ν_{12}=1/3. The lamina specimen is subjected to a velocity boundary condition of v=1 mm/min at the bottom and top edges. The peridynamic model discretization of the experimental setup is created by using a single material-point layer with a grid size of Δx=0.403 mm and the size of the horizon is specified as $\delta = 3.015\Delta x$.

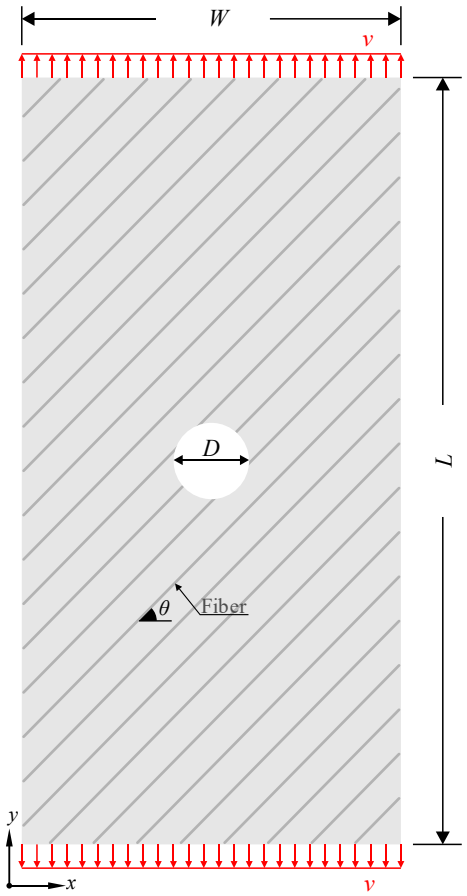

Fig. 8 Experimental setup of the unidirectional composite lamina with a central hole under tensile load considered in the study of Shang et al. [39]

As shown in Fig. 9, the crack propagation pattern results are parallel with the relevant fiber orientation and almost identically matches with the experimental results (see Fig. 10) presented in the study of [39]. These results successfully confirm that the present peridynamic

model can accurately predict the damage states of unidirectional fiber-reinforced composite lamina with 0°, 45°, and 90° fiber angles.

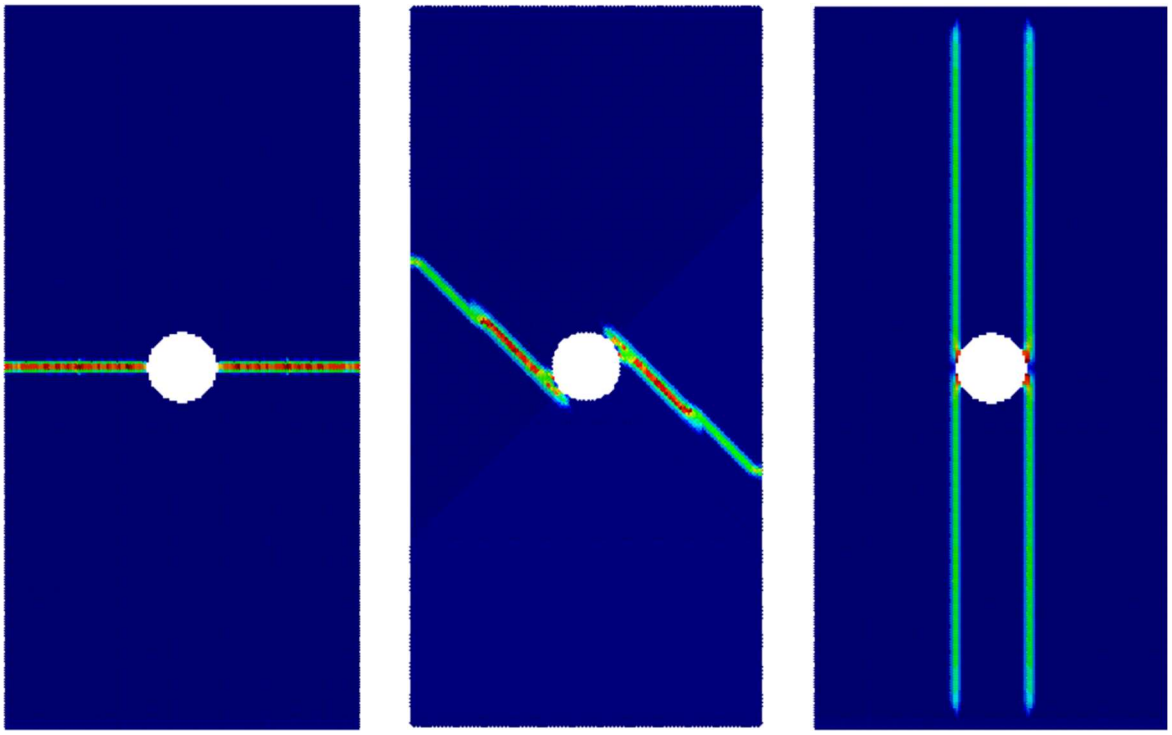

Fig. 9 Crack propagation results of peridynamic analysis for (a) 0°, (b) 45° and (c) 90° fiber orientations

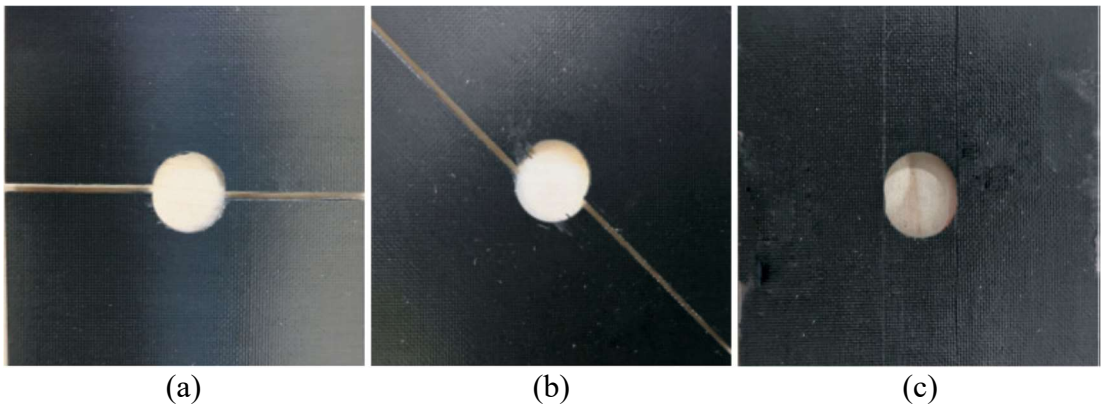

Fig. 10 Experimental crack propagation results for a composite lamina with a central hole under tensile load for (a) 0°, (b) 45° and (c) 90° fiber orientations[39]

4. Numerical Results

This section presents the effects of micro-cracks on toughness enhancement in composite laminae by utilizing the peridynamic model. In total, 15 different case studies are considered and analyzed by including multiple micro-cracks for three different fiber orientations of 0°, 45°, 90°. The main purpose of these cases is to demonstrate the effects of the presence of micro-cracks with various numbers or positioning on the main-crack tip strain energy density and crack extension lengths. For all cases, micro-cracks have a length of $3\Delta x$ and variations have

been created by changing the positionings and numbers of micro-cracks. As shown in Fig. 11, a rectangular composite lamina with the dimensions of $L\times W\times t$=152.4×76.2×0.1651 mm^3 having a pre-existing crack is subjected to a quasi-static tensile load in the form of velocity boundary conditions v = $1.5\cdot10^{-8}$ m/s at the bottom and top edges. The tensile load is represented as a displacement load with a constant velocity throughout the simulation. The pre-existing crack (main-crack) with a length of L_m=L/5 is perpendicular to the loading direction and positioned horizontally to the left and vertically to the middle of the lamina (see Fig. 11).

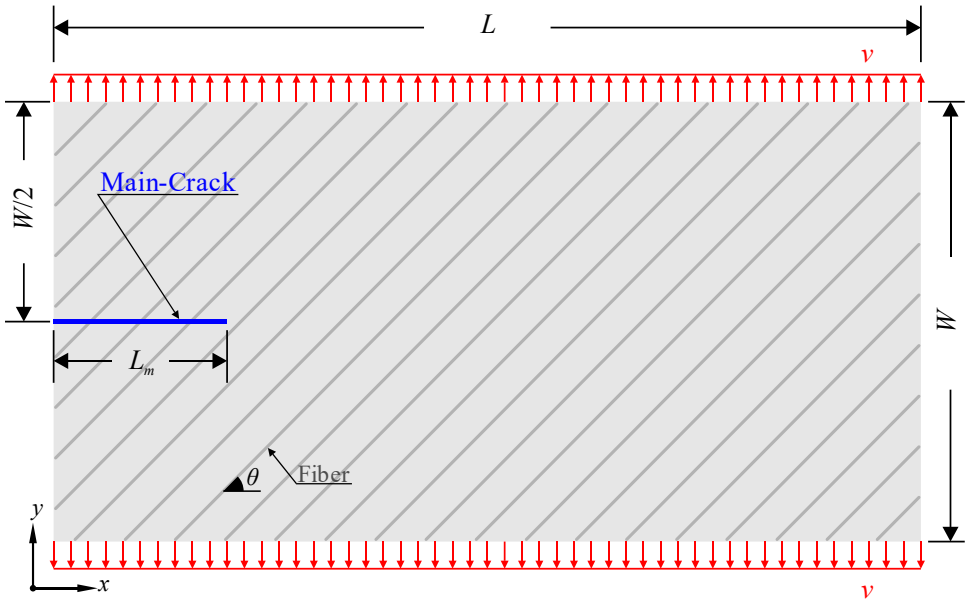

Fig. 11 Problem setup of a composite lamina subjected to quasi-static tensile load

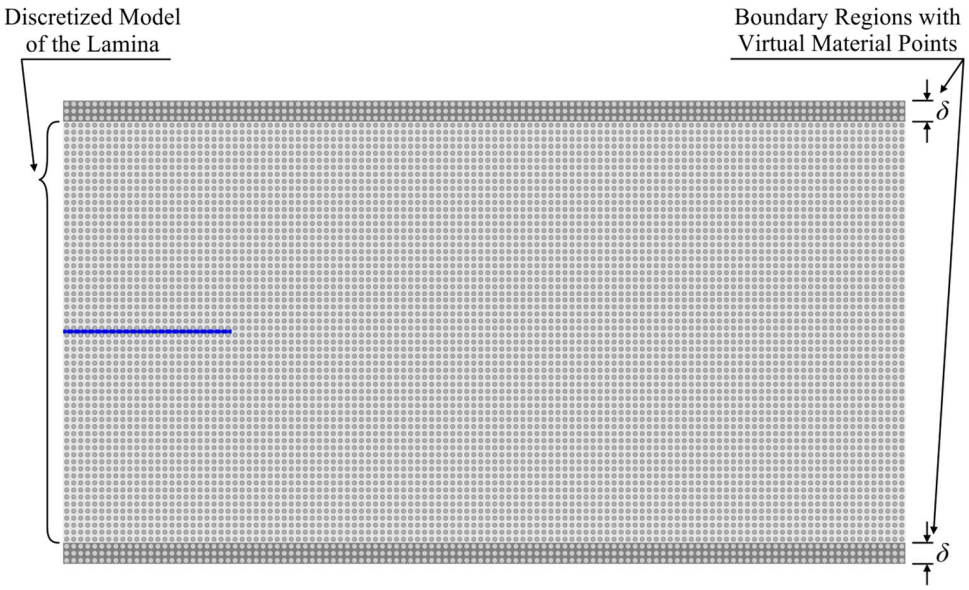

Fig. 12 Discretization of peridynamic model into 240×120×1 material points

Spatial discretization of the model is generated by using 240×120×1 material-points based on a meshless scheme (see Fig. 12). According to the discretization, the spacing of the

material points is specified as Δx = 0.635 mm and the size of the horizon is chosen as δ = 3.015Δx. As can be seen in Fig. 12, due to the non-local nature of the theory, virtual material point layers with a length equivalent to the horizon size δ are added to the top and bottom bounding lines of the model to enable a smooth and accurate boundary condition application.

The elastic moduli of the composite lamina are specified as E_1=159.96 GPa and E_2=8.96 GPa in fiber and transverse directions, respectively, and the Poisson's ratio is ν_{12}=1/3. The critical stretch values of matrix and fiber bonds, which are the fracture parameters of the material, are specified as s_m = 0.0135 and s_f = 0.027, respectively, based on the study of Oterkus and Madenci [38]. To enforce quasi-static solution, adaptive dynamic relaxation (ADR) technique is utilized in the PD analysis [58] with time increment value of 1 second and stable mass density of 7.005x10^{18} kg/m^3 [38].

4.1. Composite lamina with 0° fiber orientation

For a composite lamina with 0° fiber orientation and without micro-cracks, damage propagation continues uniformly along the main-crack direction and reaches the lamina's right edge (see Fig. 13). To postpone the main-crack's destabilization and then slow down its propagation speed, it is aimed to decelerate the increase of the strain energy density at the tip of the main-crack with the designed micro-crack patterns. The cases are designed by increasing the number of micro-cracks and revising their positions according to the obtained results. As demonstrated in Fig. 14, five cases with 12, 32, 280, 282, 754 micro-cracks are considered. In all cases, micro-cracks are positioned symmetrically with respect to the main-crack direction and their locations are designed to be in repetitive manner on the same pattern. The details of these patterns are given in Fig. 14.

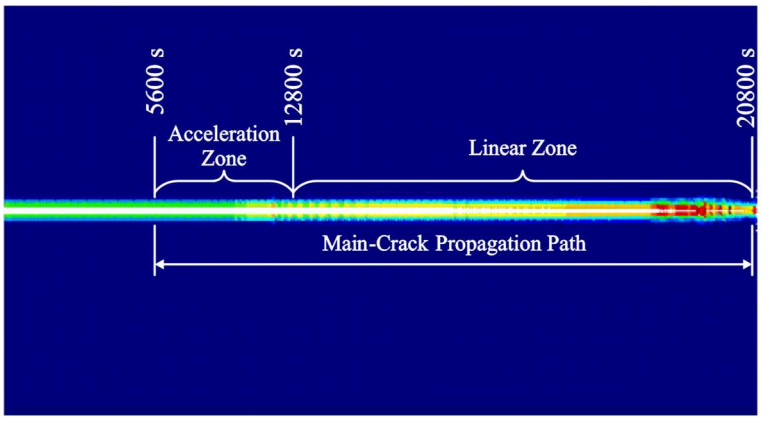

Fig. 13 Damage plot for 0° fiber orientation reference case (without micro-cracks)

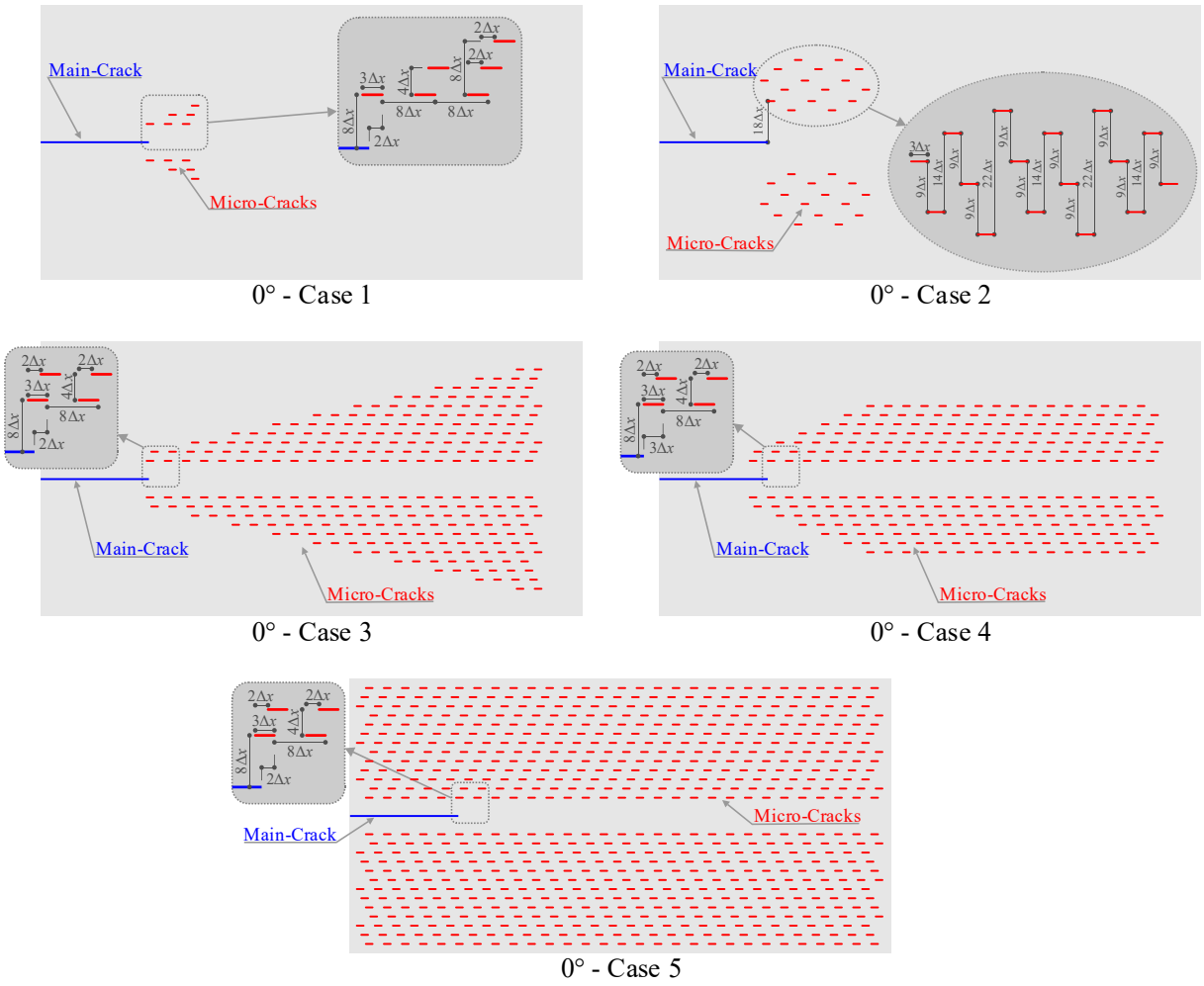

Fig. 14 Details of micro-crack positioning patterns for 0° fiber orientation cases

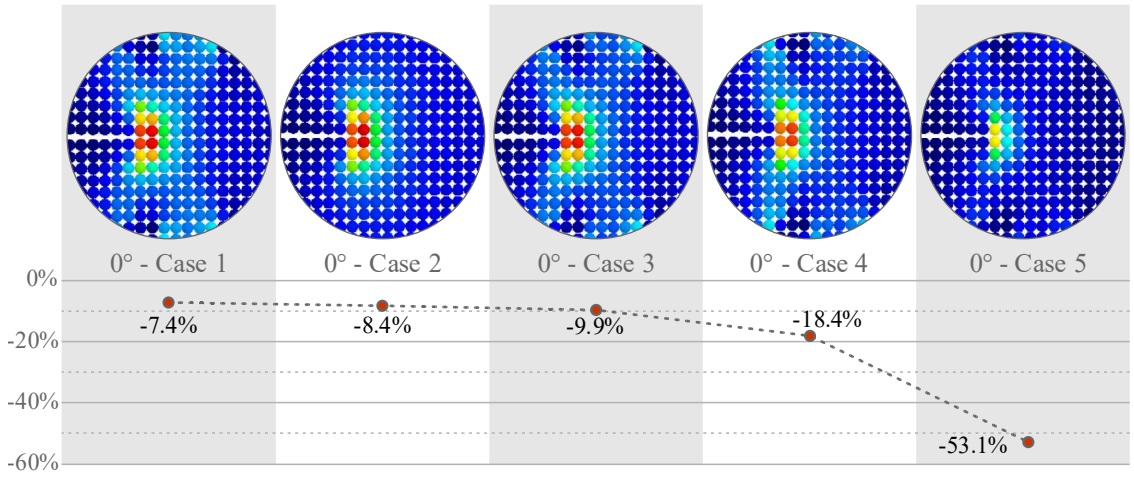

Fig. 15 Strain energy density plots and alteration graphs (%) of the main-crack tip at 5600th time step for 0° fiber orientation cases

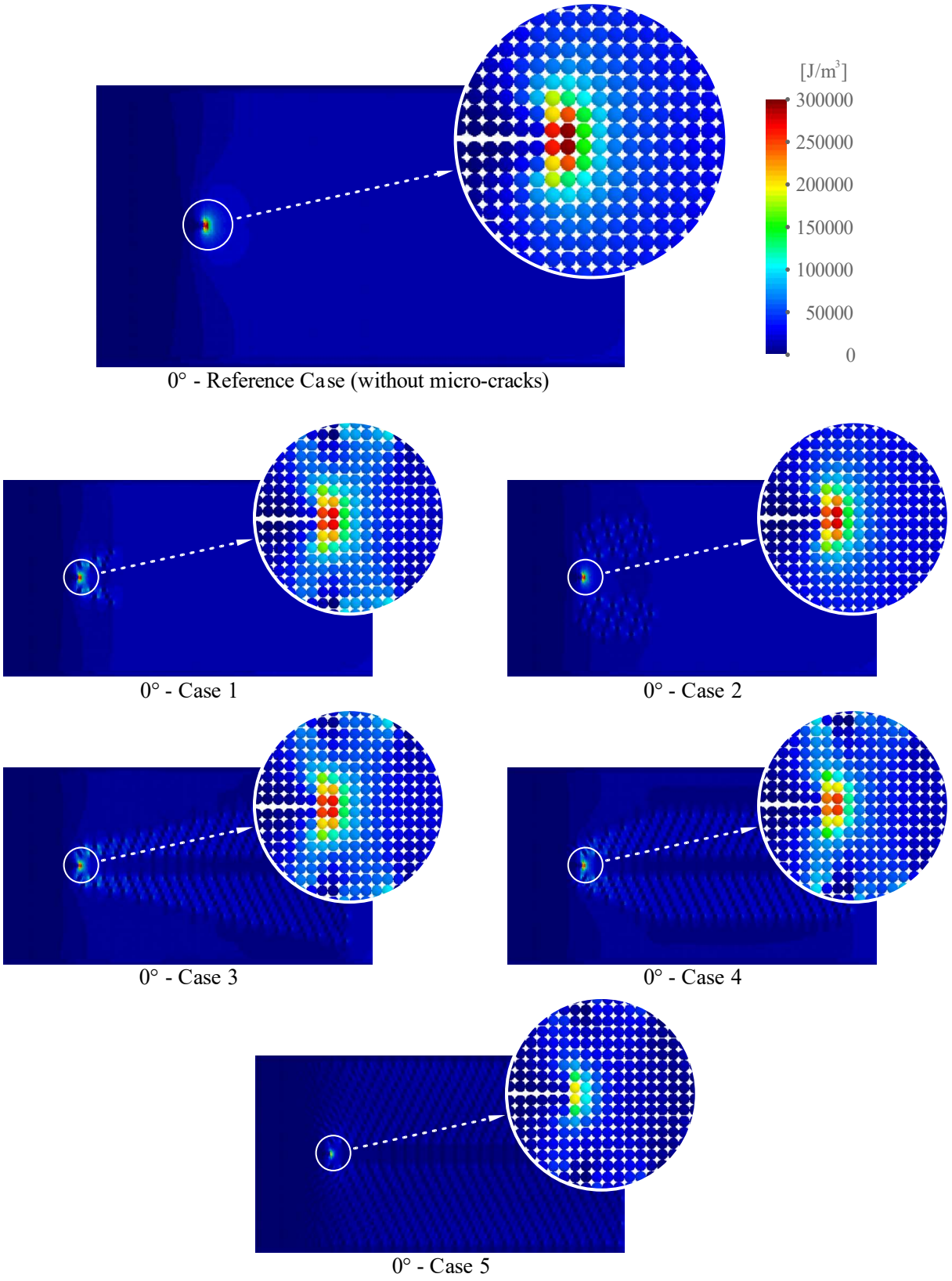

Fig. 16 Strain energy density plots at 5600th time step for 0° fiber orientation cases

First, when the micro-cracks are included, the amount of strain energy density reformation at the main-crack tip is investigated. To this end, in the case of without micro-cracks (just before the main-crack's destabilization at 5600th time step), the strain energy

density at the main-crack's tip is compared with the cases including micro-cracks for the same time step and the effects of the micro-crack patterns are evaluated accordingly. The relative change of the average strain energy density at the main-crack tip vicinity for the cases with micro-cracks are compared with the reference case without micro-cracks as shown in Fig. 15.

The obtained reduction rates in 0°-Cases 1, 2, 3 are close to each other and around -8.5% on average (see Fig. 15 & Fig. 16). On the other hand, in the 0°-Cases 4 and 5, the reduction rates change significantly by -18.4% and -53.2%, respectively (see Fig. 15 & Fig. 16). Two factors are influential in these changes including the number of micro-cracks and the presence of micro-cracks located behind the main-crack tip.

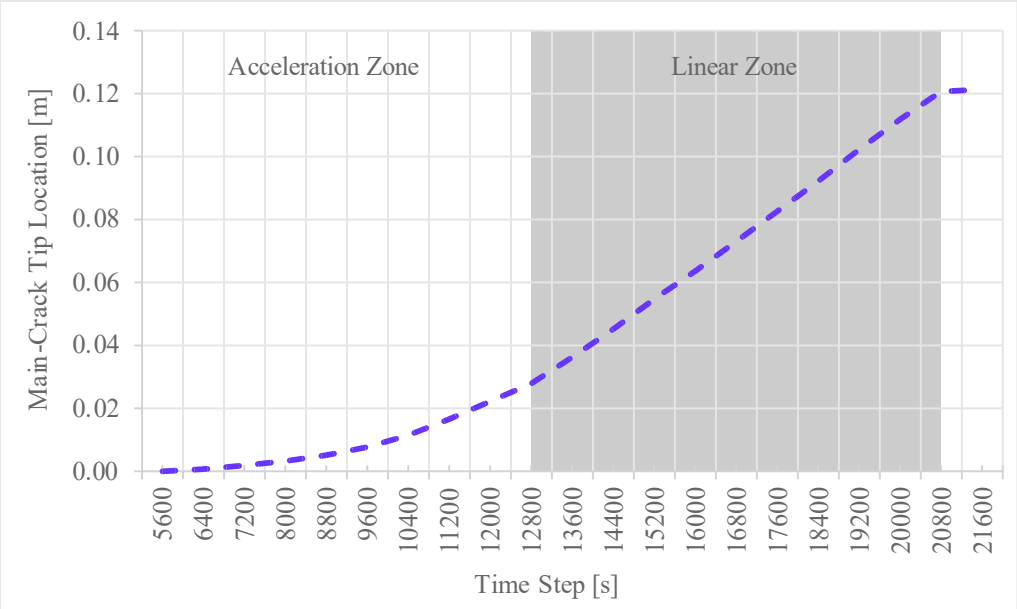

Fig. 17 The main-crack tip location graph according to the time step for 0° fiber orientation reference case (without micro-cracks)

For the first three cases, the contribution of increase in the number of micro-cracks to the change of strain energy density at the main-crack tip is at most -9.9%. What is remarkable in these ratios is the difference between the 0°-Cases 3 and 4 which is almost two times (i.e., -18.4%) although they have almost the same number of micro-cracks. For 0°-Case 4, the main factor that enables this result is the positioning of even fewer number of micro-cracks behind the main-crack tip. It can be clearly seen that this positioning strategy, which is different from the previous cases, affects this significant decrease. Finally, in 0°-Case 5, the reduction reaches up to -53.1% obtained with positioning of micro-cracks distributed throughout the lamina.

Next, the effect of micro-cracks on the position-time change of the main-crack tip in the propagation process of the main-crack is evaluated (see Fig. 18). In the position-time graph of

the reference case without micro-cracks, two major zones are observed: (i) the acceleration zone and (ii) the linear zones as depicted in Fig. 13 and Fig. 17.

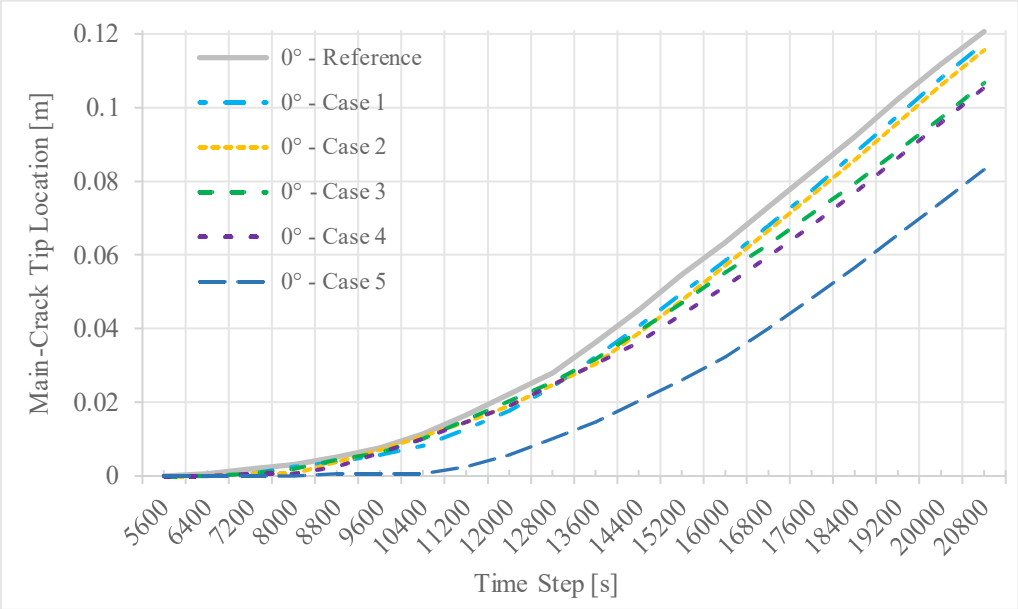

Fig. 18 The main-crack tip location graph according to the time step for 0° fiber orientation cases

For the reference case, it is observed that acceleration of the crack occurs until the 12800th time step after the start of main-crack propagation and this trend continues with an almost constant speed until the 20800th time step (see Fig. 17). After the 20800th time step, the linear trend is lost, and the rupture occurs because the main-crack tip is getting very close to the edge. Therefore, the 20800th time step of the reference case is determined as the benchmark time step. With respect to the reference case, the graph of the main-crack length changes and damage plots at the 20800th time step of all cases is presented in Fig. 19 and Fig. 20, respectively.

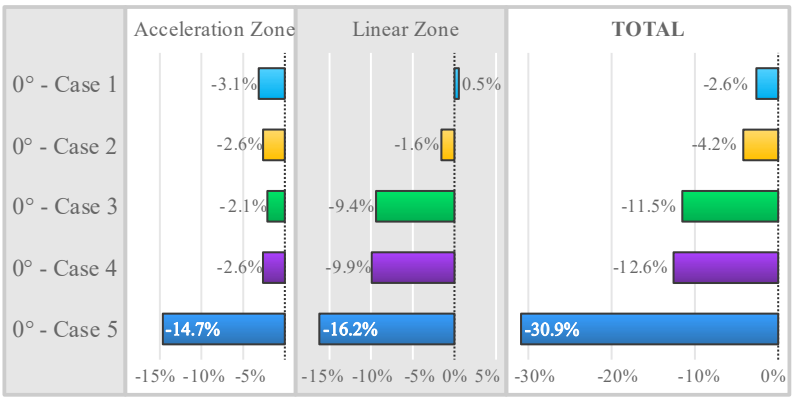

Fig. 19 The main-crack tip propagation length change graph (%) at 20800th time step for 0° fiber orientation cases

In the first two cases in which micro-crack positioning focused on the main-crack tip initially, the main-crack length is decreased by -3.4% on average (see Fig. 19). In the third and

fourth cases where the positioning is expanded along the main-crack path, the decrease in the main-crack length is around -12% on average (see Fig. 19). In the last case with micro-crack positioning covering the entire lamina, the decrease in the main-crack length reaches up to -31% (see Fig. 19).

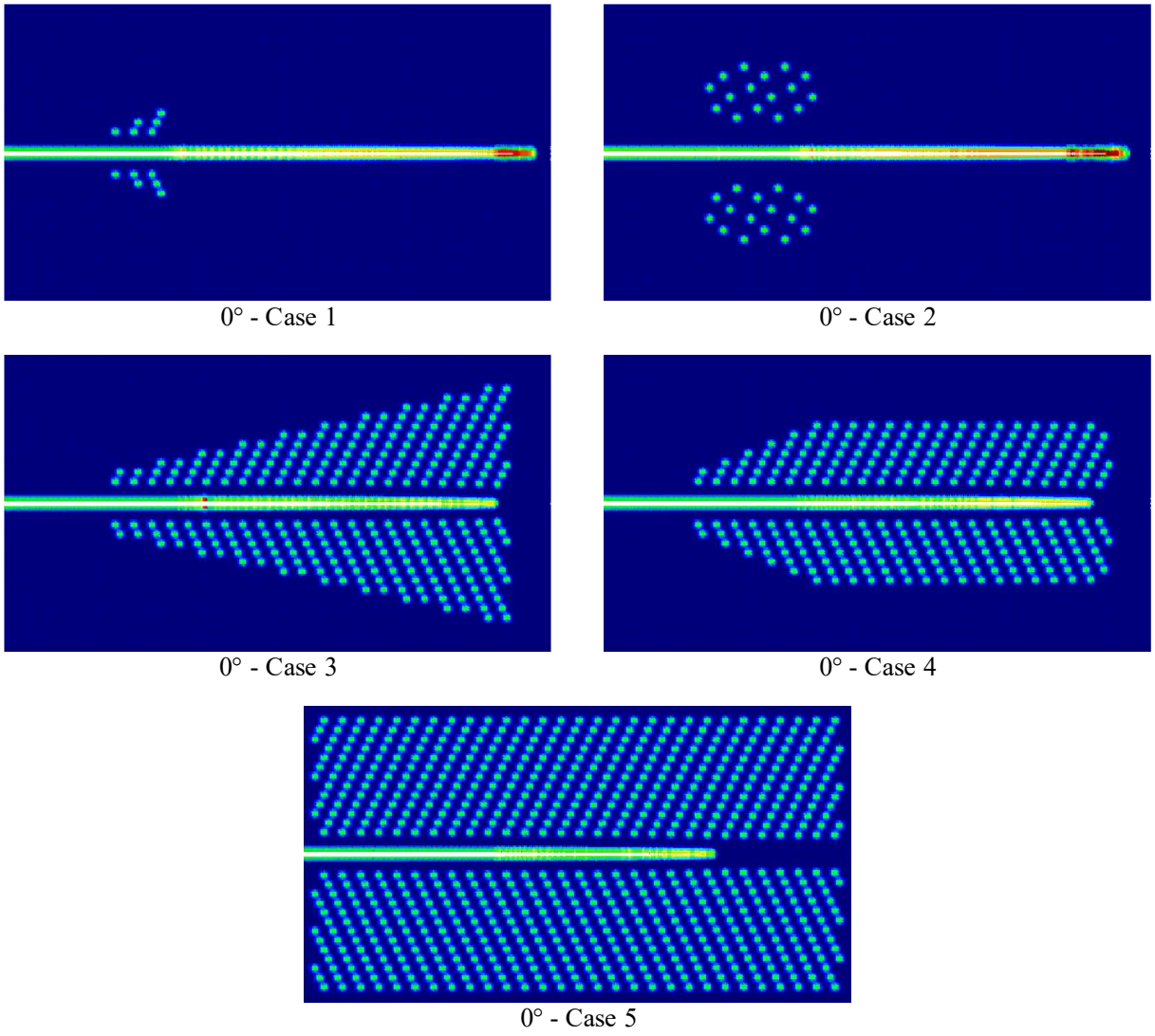

Fig. 20 Damage plots at 20800th time step for 0° fiber orientation cases

In Fig. 19, the main-crack length changes are presented separately for both the acceleration and the linear zones to evaluate the effects of micro-crack patterns on the entire propagation period. In the first two cases in which micro-crack positioning focused on the main-crack tip initially, almost all of the decrease in the main-crack length occurs until the end of the acceleration zone. In the third and fourth cases, the distribution of these shortening rates in the acceleration and linear zones are -2.4% and -9.7% on average, respectively. In the last case, this distribution occurs as -14.7% and -16.2%.

As a result, widespread micro-crack positioning along the propagation path significantly enhances the toughness. Even though the micro-crack positionings behind the main-crack tip are very efficient to postpone the initiation of the main-crack, it has a limited effect on the main-crack final propagation length.

4.2. Composite lamina with 45° fiber orientation

For a composite lamina with 45° fiber orientation and without micro-cracks, damage propagation continues along the fiber direction and reaches the lamina's top edge (see Fig. 21). It is aimed to decelerate the increase of the strain energy density at the tip of the main-crack with the designed micro-crack patterns to postpone the main-crack's destabilization and then slow down its propagation speed. By increasing the number of micro-cracks and revising their positions, the cases are designed according to the obtained results. As detailed in Fig. 22, five cases with 26, 43, 67, 91, 105 micro-cracks are investigated. In all cases, the micro-cracks positioning is in the form of a repetition of the same pattern, so only the dimensions of the pattern are given in Fig. 22.

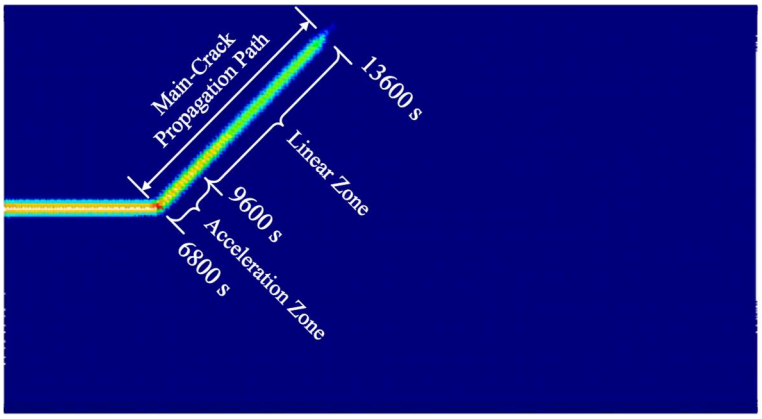

Fig. 21 Damage plot for 45° fiber orientation reference case (without micro-cracks)

First, the strain energy density changes at the main-crack tip are examined when micro-cracks are included. For the reference case without micro-cracks, just before the main-crack's destabilization (at 6800th time step), the strain energy density at the main-crack's tip is compared with the cases including micro-cracks for the same time step, and the effects of the micro-crack patterns are examined. As seen in Fig. 23, the relative change of the average strain energy density at the main-crack tip for the micro-crack included cases are compared with the reference case without micro-cracks. Although for 45°-Cases 3,4,5, there is a reduction of -20.3% on average, for 45°-Cases 1 and 2, there is an increase of 12.2% on average (see Fig. 23 & Fig. 24). The main factor that causes increasing and decreasing groups among the results are directly related to whether micro-crack positioning is on both sides of the main-crack

propagation path. The presence of micro-cracks on both sides of the main-crack propagation path provides balance in reciprocal fiber stresses, and the contribution of micro-cracks to the decrease in the strain energy density at the main-crack tip vicinity is revealed.

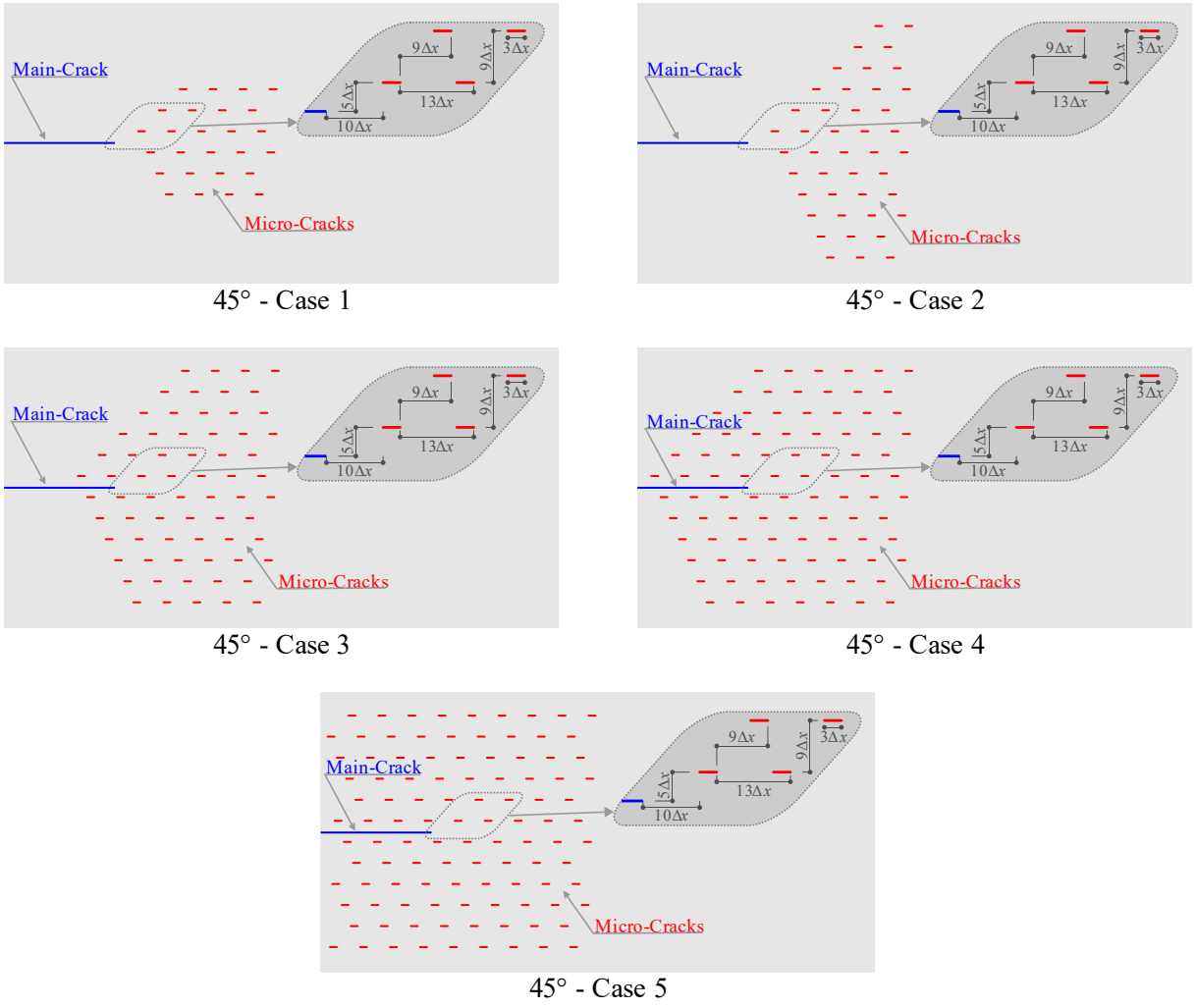

Fig. 22 Micro-crack positioning patterns and dimensioning details for 45° fiber orientation cases

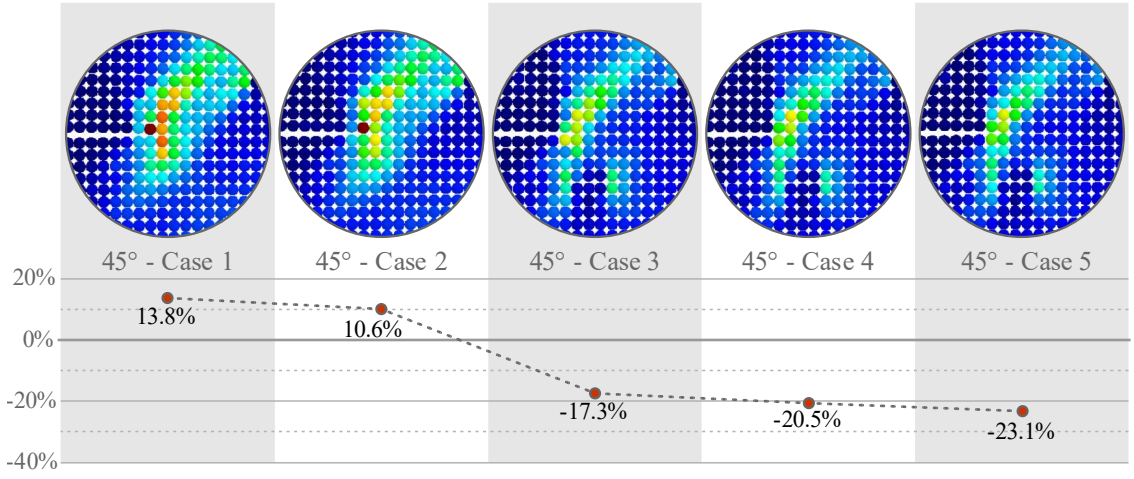

Fig. 23 Strain energy density plots and alteration graphs (%) of main-crack tips at 6800th time step for 45° fiber orientation cases

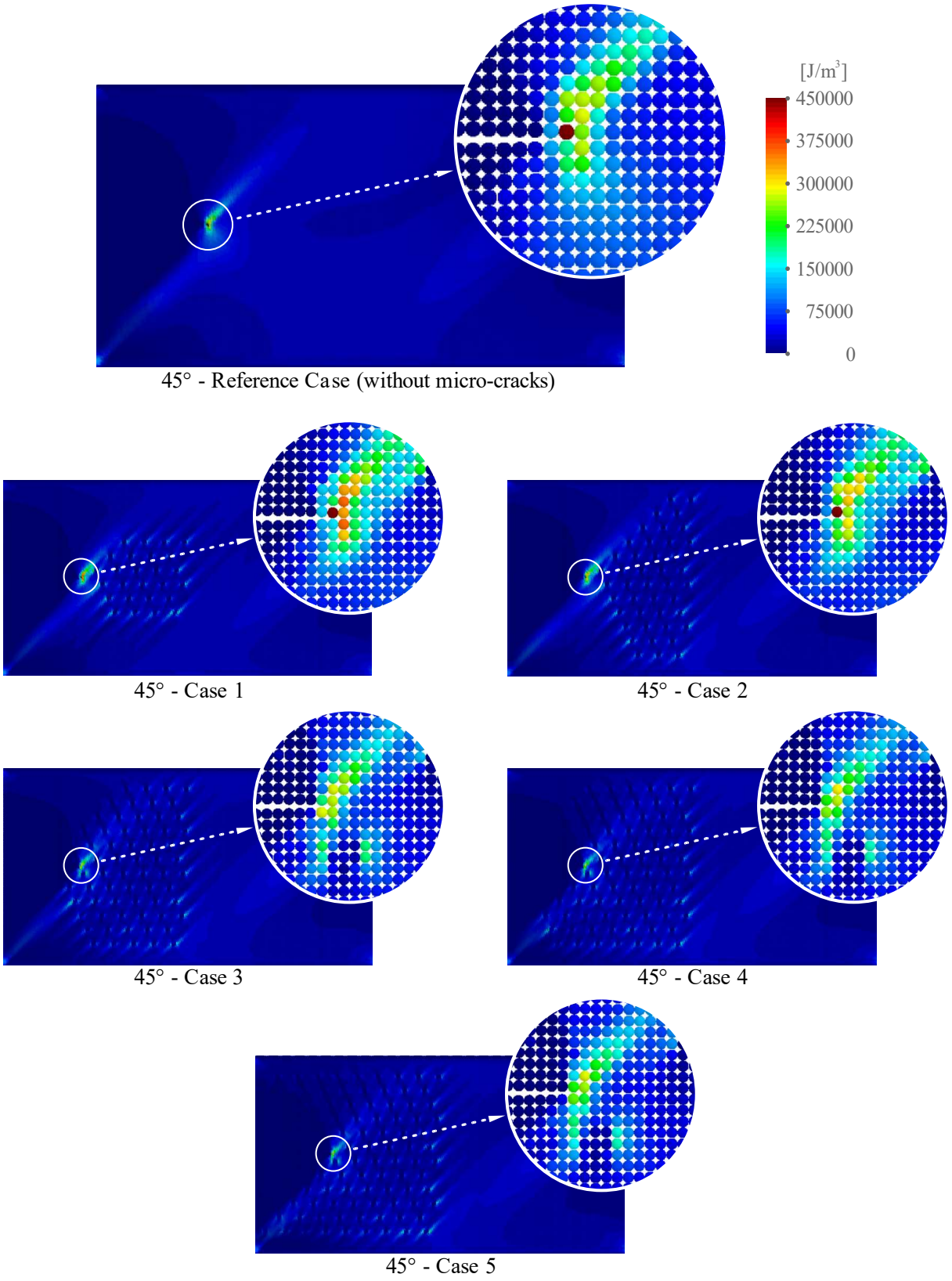

Fig. 24 Strain energy density plots at 6800th time step for 45° fiber orientation cases

In the first two cases, due to the micro-cracks, the load required to be carried by the ruptured fibers is redistributed to adjacent fibers, which also adds additional load to the vicinity matrix. Therefore, the main-crack tip matrix strain energy density increases. In the second case,

when the number of micro-cracks is increased, the energy concentration in the fibers begins to dissipate partially and the main-crack tip matrix strain energy density decreases slightly compared to the first case. However, it is still 10.6% more than the reference case.

Subsequently, the effect of micro-cracks on the position-time change of the main-crack tip in the propagation process of the main-crack is evaluated (see Fig. 26). In the position-time graph of the reference case without micro-cracks, two major zones are observed; namely the acceleration and the linear zones (see Fig. 21 & Fig. 25).

In the reference case, the main-crack propagation speed increases until the 9600th time step, then continues at an almost constant speed (see Fig. 25). Around 13600th time step, the constant speed trend is disrupted as the main-crack approaches the top edge of the lamina (see Fig. 25). Therefore, the 13600th time step of the reference case is determined as the benchmark time step. With respect to the reference case, the graph of the main-crack length changes and damage plots in the 20800th time step of all cases are presented in Fig. 27 and Fig. 28, respectively.

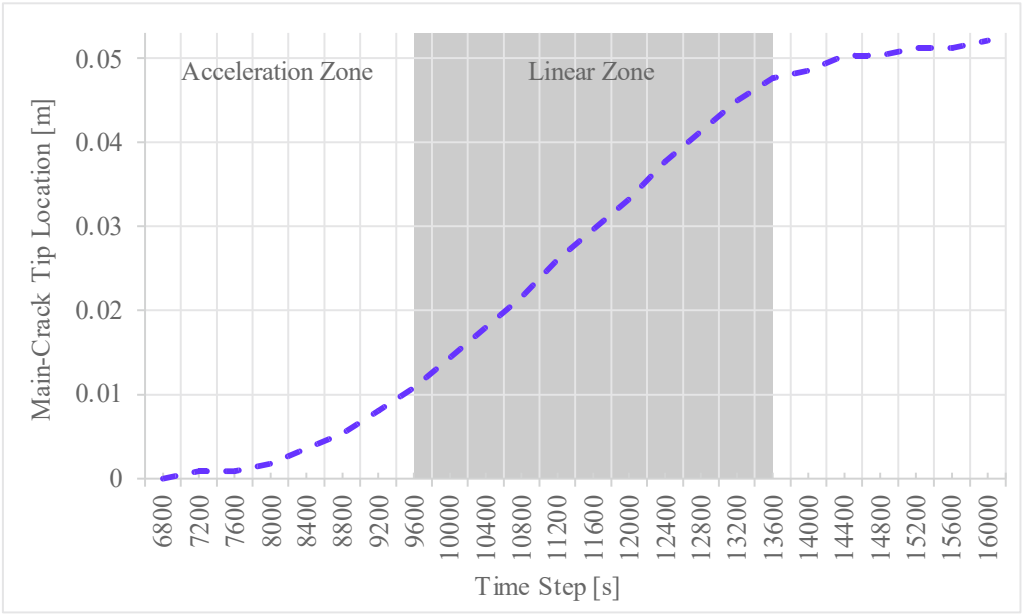

Fig. 25 The main-crack tip location graph according to the time step for 45° fiber orientation reference case (without micro-cracks)

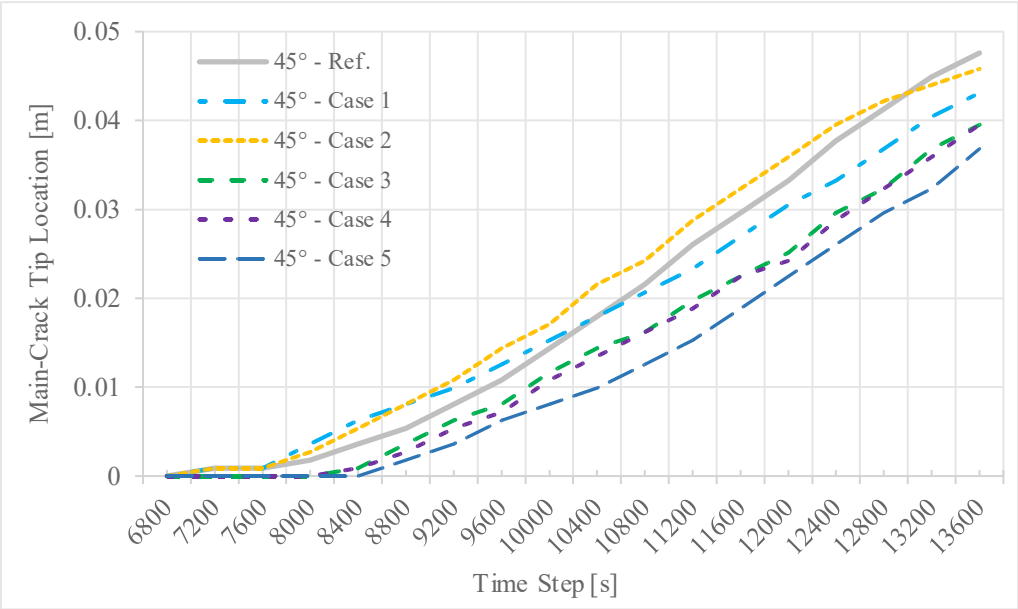

Fig. 26 The main-crack tip location graph according to the time step for 45° fiber orientation cases

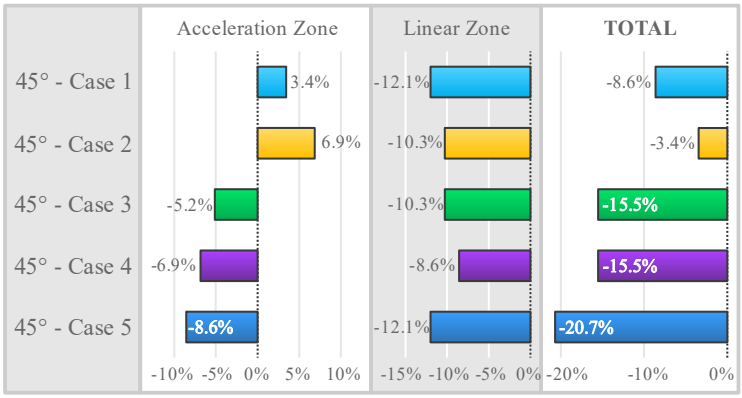

Fig. 27 The main-crack tip propagation length change graph (%) at 13600th time step for 45° fiber orientation cases

In the first two cases (45°-Cases 1 and 2), all micro-cracks are placed below the main-crack propagation path. In these two cases (45°-Cases 1 and 2), the main-crack propagation speed is faster than the reference case while passing nearby the micro-cracked region, and gets slower than the reference case by the end of these regions, which result in a decrease in the final main-crack length by -8.6% and -3.4%, respectively. The regional accelerations are due to the disruption of the fiber balance on both sides of the main-crack propagation path by the micro-cracks. In the subsequent three cases (45°-Cases 3, 4, 5), the micro-crack regions are expanded to above and behind the main-crack propagation path to achieve this balance, and as a result, -17.2% on average reduction in the main-crack length is achieved.

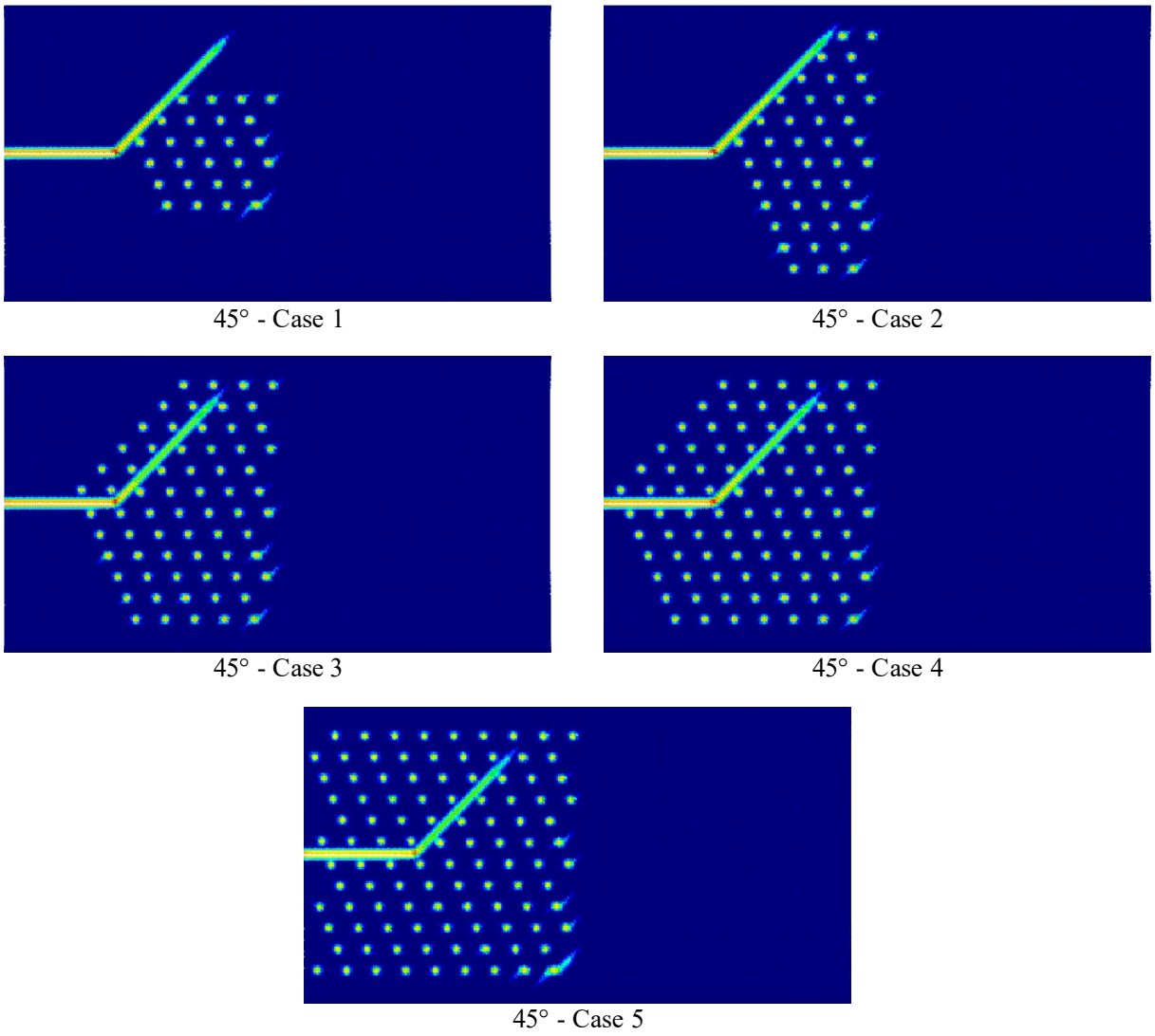

Fig. 28 Damage plots at 13600th time step for 45° fiber orientation cases

For the first two cases, initially, the main-crack propagation is faster than the reference case since the balance of micro-cracks on both sides of the main-crack propagation path is not satisfied. Later, recovery occurs in these losses, and the main-crack length reduction is obtained in the 13600th time step. For the other three cases, the main-crack's propagation is delayed by 1200 to 1600 time steps, and after propagation starts, these cases have similar propagation trends with respect to each other. As a result, the balanced micro-crack positioning on both sides of the main-crack propagation path eliminates this undesirable effect. In addition, the micro-crack positioning to be made behind the main-crack tip is remarkably effective in delaying the main-crack propagation.

4.3. Composite lamina with 90° fiber orientation

For a composite lamina with 90° fiber orientation and without micro-cracks, damage propagation continues along the fiber direction in both ways, namely downwards and upwards,

and reaching to the lamina's lower and upper edges (see Fig. 29). For the reference case without micro-cracks, the main-crack propagation speed increases until the 6400th time step, and then a downtrend of the speed occurs, unlike other orientations.

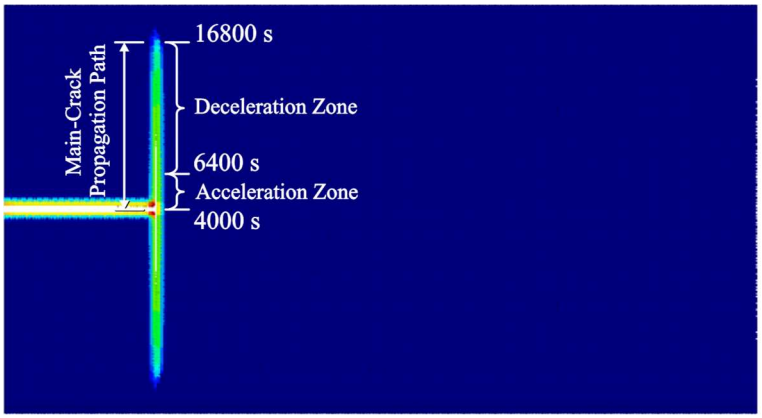

Fig. 29 Damage plot for 90° fiber orientation reference case (without micro-cracks)

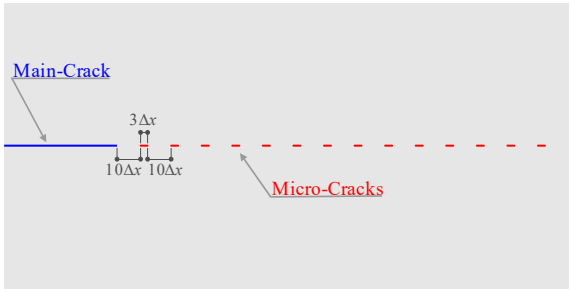

90° - Case 1

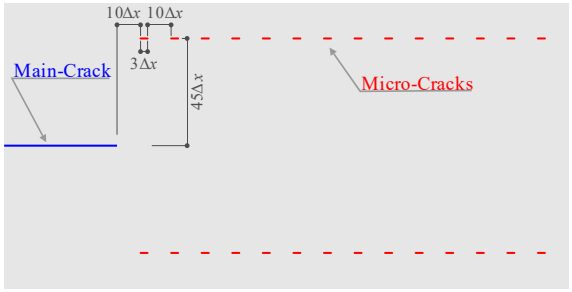

90° - Case 2

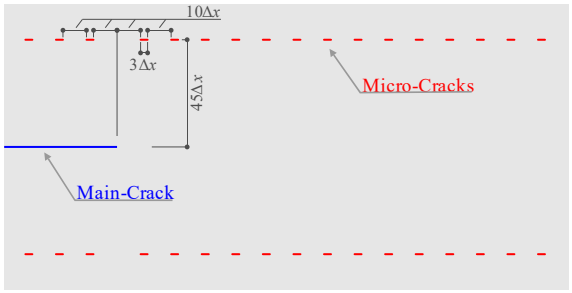

90° - Case 3

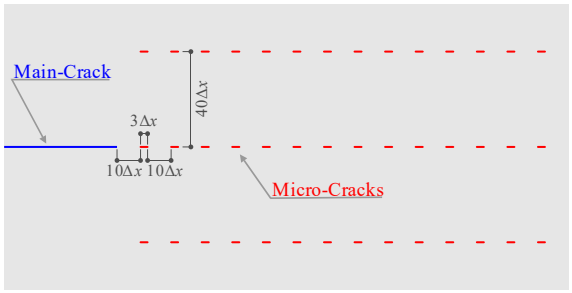

90° - Case 4

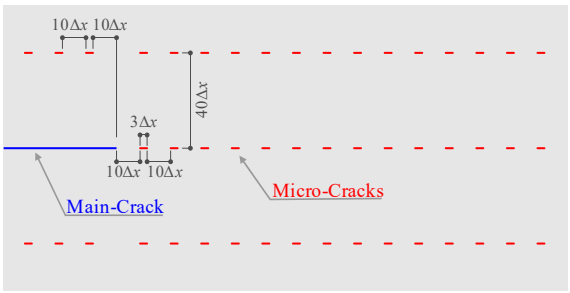

90° - Case 5

Fig. 30 Micro-crack positioning patterns and dimensioning details for 90° fiber orientation cases

To postpone the main-crack's destabilization, it is aimed to decelerate the increase of the strain energy density at the tip of the main-crack with the designed micro-crack patterns. As detailed in Fig. 30, five cases with 14, 28, 34, 42, 48 micro-cracks are considered. In all cases, micro-cracks are symmetrical to the main-crack direction and their positioning is in the form of a repetition of the same pattern, so only the dimensions of the pattern are given in Fig. 30.

First, the strain energy density changes at the main-crack tip are evaluated when micro-cracks are included. In the case without micro-cracks, just before the main-crack's destabilization (at 4000th time step), the strain energy density at the main-crack's tip is compared with the cases which included micro-cracks for the same time step, and the effects of the micro-crack patterns are evaluated. As seen in Fig. 31, the relative change of the average strain energy density at the main-crack tip vicinity of the cases with micro-cracks are compared with the reference case without micro-cracks.

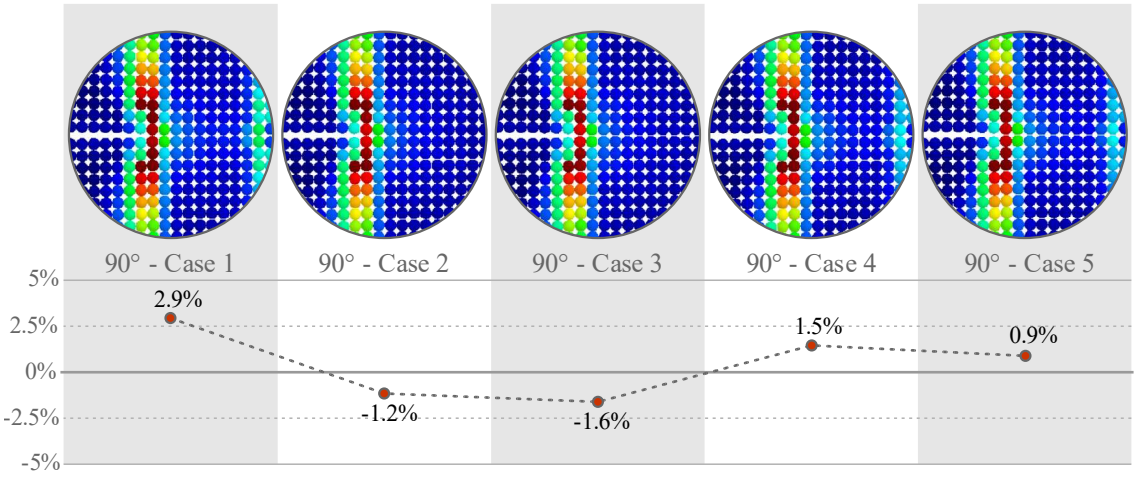

Fig. 31 Strain energy density plots and alteration graphs (%) of main-crack tips at 4000th time step for 90° fiber orientation cases

The contribution of the micro-cracks is limited to reduce the main-crack tip strain energy densities and, even in some cases, causes to increase. According to the results, for 90°-Cases 2 and 3, there is a decrease of -1.4% on average, while for the other three cases, an increase between 0.9% and 2.9% occurs (see Fig. 31 & Fig. 32). In these three cases, the load required to be carried by the ruptured fibers is redistributed to adjacent fibers due to the micro-cracks near the main-crack tip. This also adds additional load to the matrix in the close vicinity. Therefore, the strain energy density of the main-crack tip increases.

Due to the coincidence of the fiber orientation and the loading direction, the micro-cracks are insufficient to reduce the strain energy density of the main-crack tip. Therefore, the fiber-matrix debonding occurs readily at the boundaries of fiber bundles broken by the micro-cracks

(see Fig. 33). The micro-cracks yield new crack propagations instead of reducing main-crack tip energy density and thus cause more damage to the lamina.

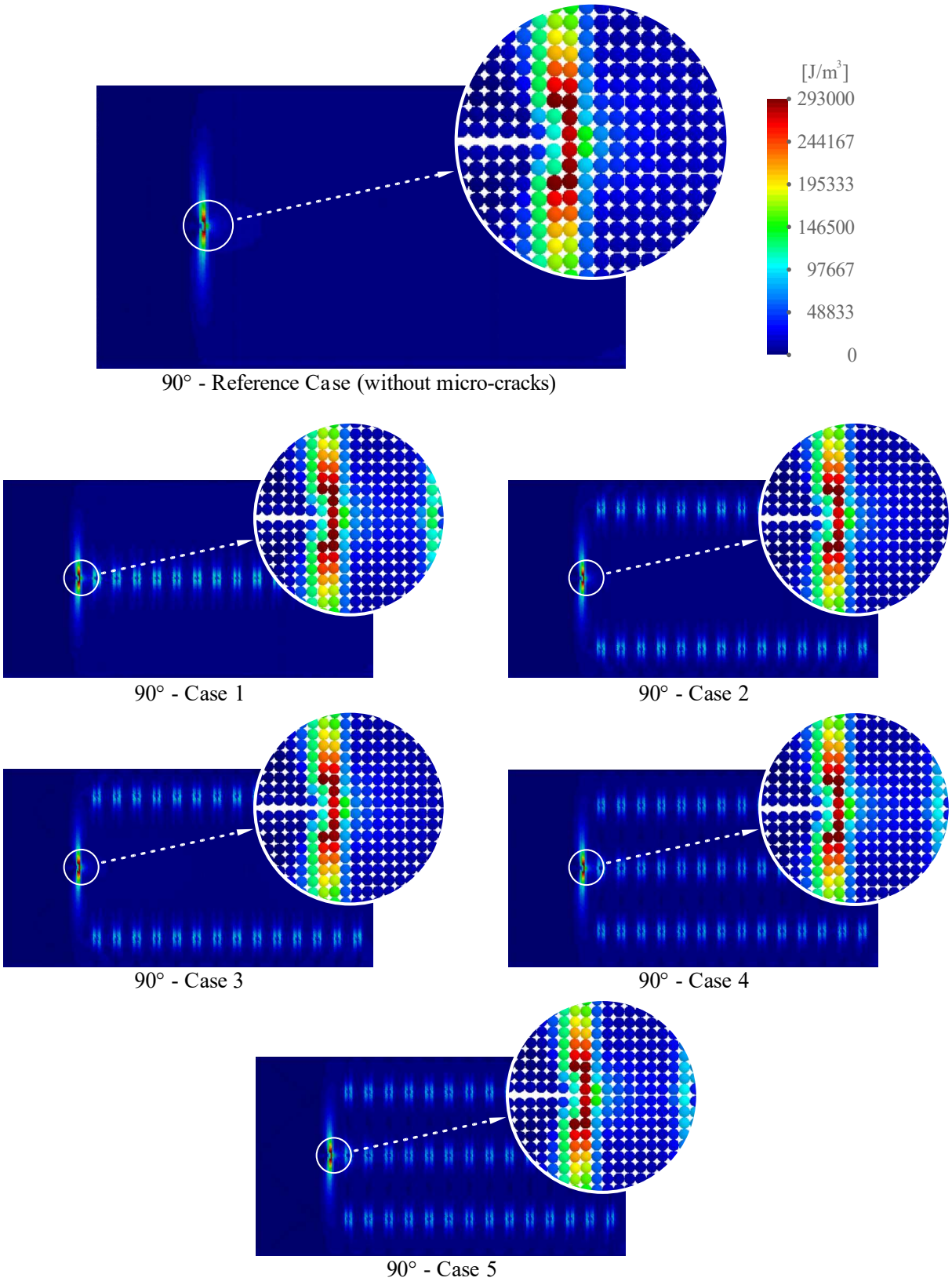

Fig. 32 Strain energy density plots at 4000th time step for 90° fiber orientation cases

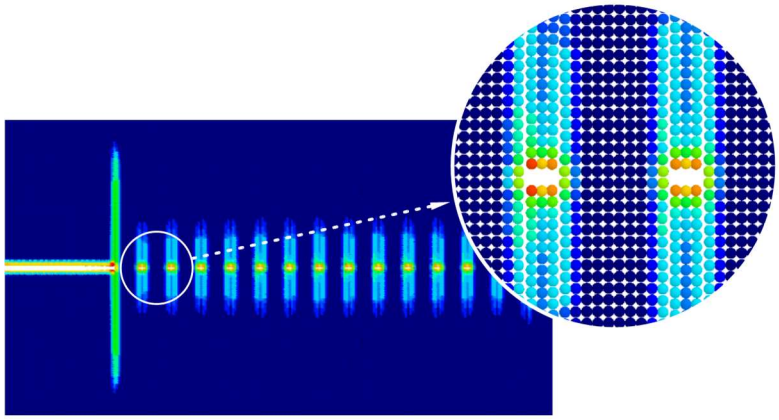

Fig. 33 Fiber-matrix stripping initiating at micro-crack tips in 90° fiber orientation case

Subsequently, the effect of micro-cracks on the position-time change of the main-crack tip in the propagation process of the main-crack is evaluated (see Fig. 35). In the position-time graph of the reference case without micro-cracks, two major zones are observed; namely the acceleration and the deceleration zones (see Fig. 29 & Fig. 34). In the reference case, the main-crack propagation speed increases until the 6400th time step then starts to decelerate (see Fig. 34). Around the 16800th time step, pauses occur on propagation as the main-crack approaches the top and bottom edges of the lamina (see Fig. 34). Therefore, the 16800th time step of the reference case where these pauses start is determined as the benchmark time step.

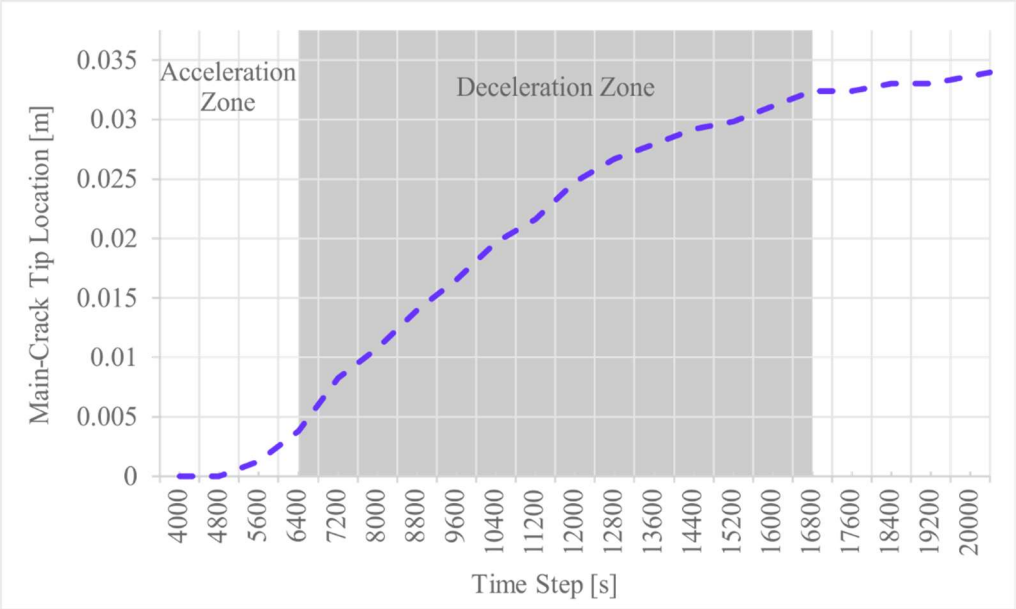

Fig. 34 The main-crack tip location graph according to the time step for 90° fiber orientation reference case (without micro-cracks)

With respect to the reference case, the graph of the main-crack length changes and damage plots in the 16800th time step of all cases are presented in Fig. 36 and Fig. 37, respectively. There is no reduction in the final main-crack length in the acceleration zones of

all cases, unlike the other orientation results, and at last, all the reductions occur in the deceleration zones. The reason for these reductions is that damage initiated from the micro-cracks is more than the main-crack propagation between 619% and 935% (see Fig. 38).

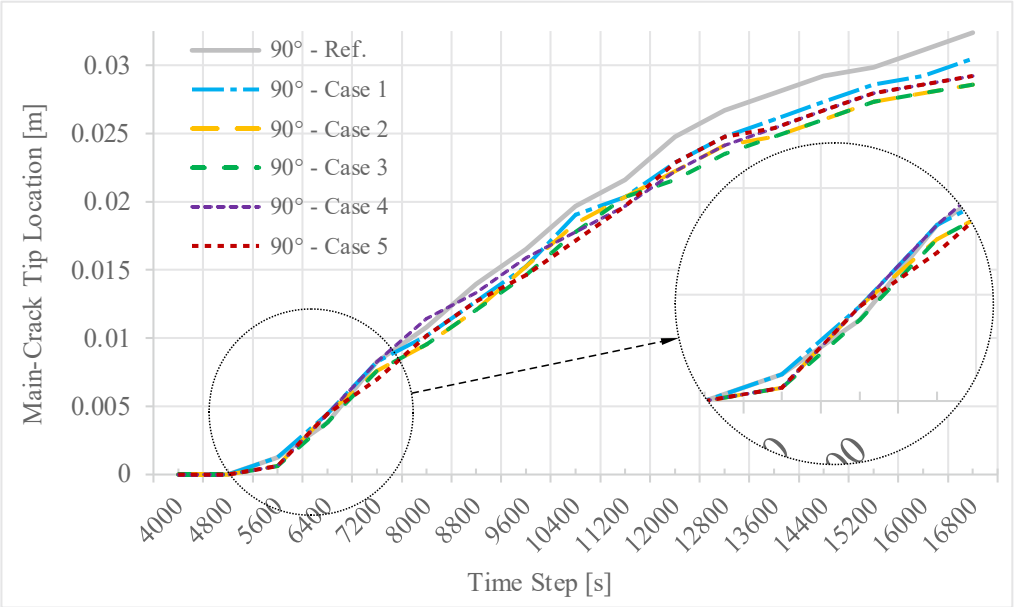

Fig. 35 The main-crack tip location graph according to the time step for 90° fiber orientation cases

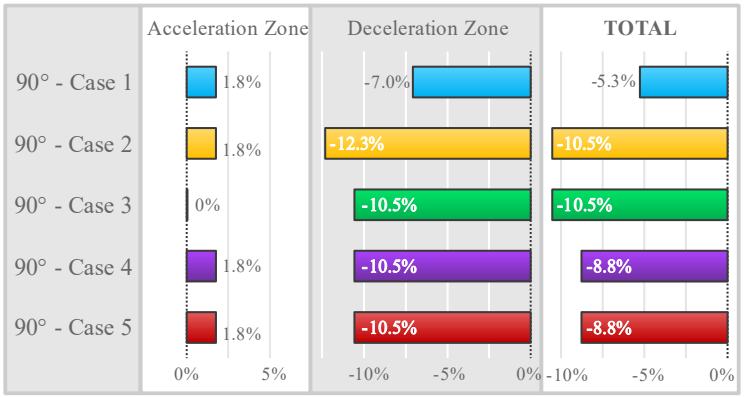

Fig. 36 The main-crack tip propagation length change graph (%) at 16800th time step for 90° fiber orientation cases

At the 8800th time step, the number of damaged material points due to the micro-cracks for all cases is on average 220% higher than the reference case (see Fig. 38). When it comes to the 16800th time step, this percent reaches 840% on average (see Fig. 38). The reduction in the main-crack length occurs as a result of the energy absorption of the widespread damages caused by micro-cracks. It does not seem possible to conclude that toughness is achieved with the decrease in the length of the main-crack caused by the damage at levels that threaten the lamina integrity. By increasing the number of micro-cracks, the general damage rises further and herewith moved away from the desired purpose gradually. As a result, it turns out that increasing the toughness by micro-cracks is not effective in 90° fiber orientation.

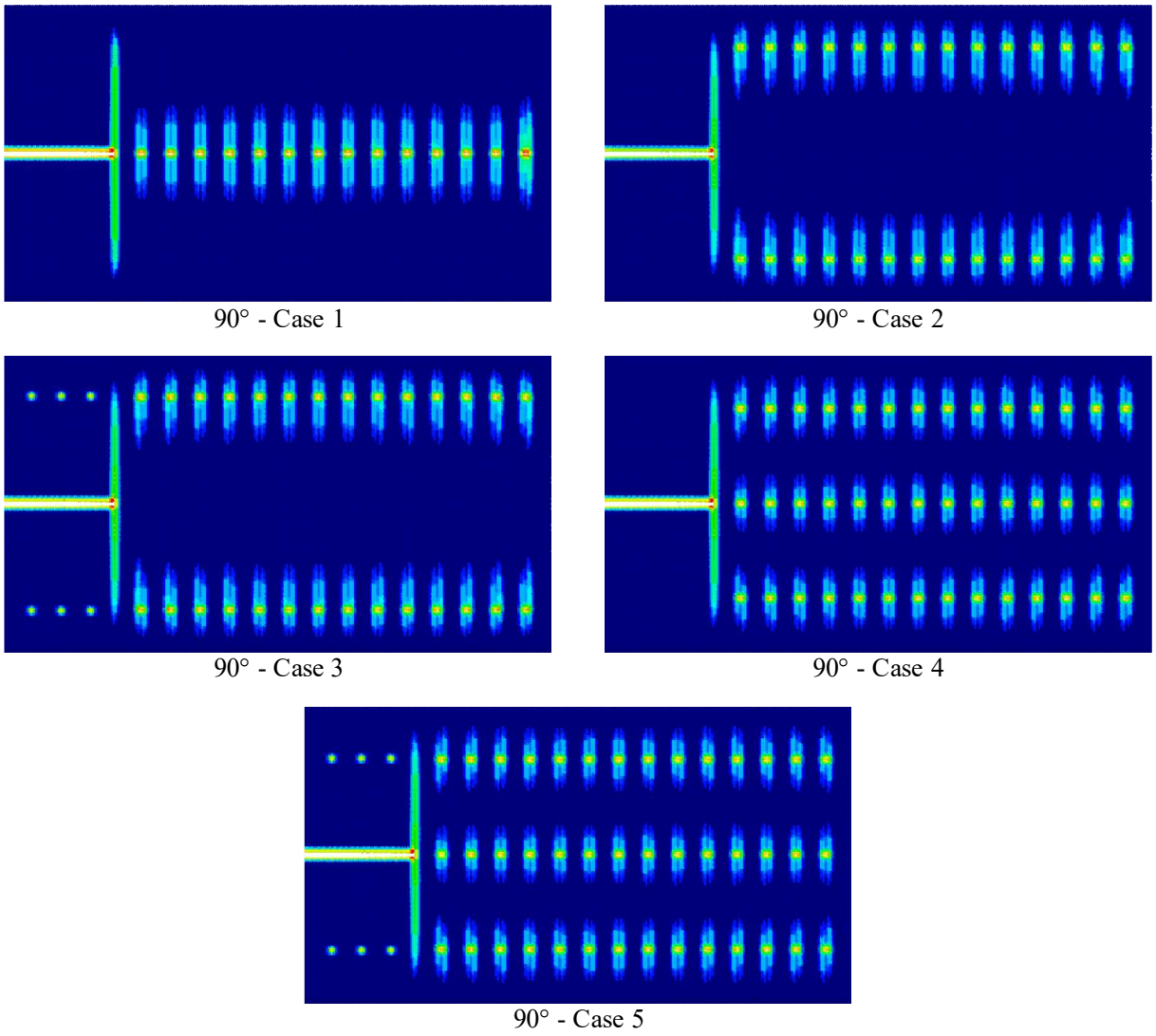

Fig. 37 Damage plots at 16800th time step for 90° fiber orientation cases

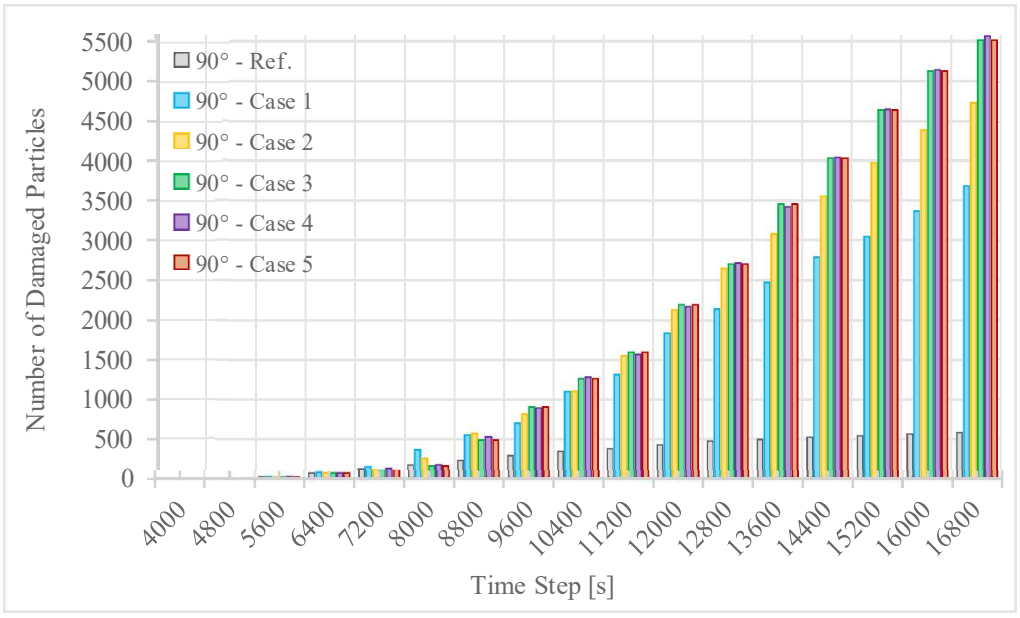

Fig. 38 Number of the damaged-material points graph according to the time step for 90° fiber orientation cases

5. Conclusion

In this research effort, the toughness enhancement strategy by micro-cracks is developed for composite laminae with various fiber orientations. To this end, a peridynamic-based computational lamina model is adopted, implemented, and verified/validated with respect to experimental/numerical results. For finding out the most effective toughness enhancement strategy for composite materials, more than 200 analyses have been conducted for the presented cases. In fact, performing this number of test cases through an experiment may be too costly, therefore the present cases are analyzed numerically thanks to the consistency and reliability of peridynamics for fracture analysis. Hence, this study reveals the advantages of the PD for developing novel toughening mechanisms.

According to the simulation results, in the presence of any damage/crack, the crack propagates promptly parallel to the fiber direction along the weak matrix interface in composites. Therefore, inclined micro-crack variations are observed to unsuitable for deflecting and branching the main-crack for composite laminae. Consequently, it is aimed to provide more elasticity to the lamina by orienting the micro-cracks perpendicular to the loading direction to get benefit from their opening-mode performances as much as possible. Based on the evaluated results, it is indicated that the micro-cracks can enhance the toughness for 0° and 45° fiber orientation cases whereas they do not play a critical role for toughening of 90° laminae. It is demonstrated that the use of micro-cracks for 90° fiber orientation cases yields to the propagation of more micro-cracks. This causes a damage level much higher than 90° lamina without micro-crack. Essentially, for 90° fiber orientation test cases, the fiber bundles are broken since the micro-cracks are stripped off the matrix interface in blocks due to action of direct loads along fiber direction.

On the other hand, for the other two orientations (0° and 45°), delay in the destabilization moment of the main-crack tip is achieved by leveraging properly positioned horizontal micro-cracks, thereby bestowing the PD composite model for toughness enhancement in composite materials. Since the fiber orientation and the loading direction do not coincide for 0°- and 45°-fiber orientations, micro-cracks can increase the strain energy dissipation. Thus, this delays complete breakage time and slowing the crack propagation speed of the main-crack. All in all, it can be concluded that the micro-cracks can contribute to the toughness enhancement of 0° and 45° laminae under opening mode of a main-crack. Overall, present PD composite model can be utilized as a viable simulation/analysis platform to substitute for experimental tests to design effective toughening mechanics of composite laminae. In future studies, an integrated

solution can be put forward where the positioning of micro-cracks is ensured by optimization techniques and analyzes can be carried out using the proposed PD composite model.

Data Availability

The raw/processed data required to reproduce these findings cannot be shared at this time as the data also forms part of an ongoing study.

References

[1] Ravi-Chandar K, Yang B. On the role of microcracks in the dynamic fracture of brittle materials. Journal of the Mechanics and Physics of Solids. 1997;45:535-63.

[2] Bleyer J, Roux-Langlois C, Molinari J-F. Dynamic crack propagation with a variational phase-field model: limiting speed, crack branching and velocity-toughening mechanisms. International Journal of Fracture. 2017;204:79-100.

[3] Kachanov M. On crack-microcrack interactions. International Journal of Fracture. 1986;30:R65-R72.

[4] Brencich A, Carpinteri A. Stress field interaction and strain energy distribution between a stationary main crack and its process zone. Engineering Fracture Mechanics. 1998;59:797-814.

[5] Zhou T, Huang C, Liu H, Wang J, Zou B, Zhu H. Crack propagation simulation in microstructure of ceramic tool materials. Computational Materials Science. 2012;54:150-6.

[6] Li X, Li X, Jiang X. Influence of a micro-crack on the finite macro-crack. Engineering Fracture Mechanics. 2017;177:95-103.

[7] Xiaotao L, Xu L, Hongda Y, Xiaoyu J. Effect of micro-cracks on plastic zone ahead of the macro-crack tip. Journal of Materials Science. 2017;52:13490-503.

[8] Rose LRF. Microcrack interaction with a main crack. International Journal of Fracture. 1986;31:233-42.

[9] Loehnert S, Belytschko T. Crack shielding and amplification due to multiple microcracks interacting with a macrocrack. International Journal of Fracture. 2007;145:1-8.

[10] Hutchinson JW. Crack tip shielding by micro-cracking in brittle solids. Acta Metallurgica. 1987;35:1605-19.

[11] Wawersik WR, Fairhurst C. A study of brittle rock fracture in laboratory compression experiments. International Journal of Rock Mechanics and Mining Sciences & Geomechanics Abstracts. 1970;7:561-75.

[12] Bocca P, Carpinteri A, Valente S. Mixed mode fracture of concrete. International Journal of Solids and Structures. 1991;27:1139-53.

[13] Malvar LJ, Warren GE. Fracture energy for three-point-bend tests on single-edge-notched beams. Experimental Mechanics. 1988;28:266-72.

[14] Petersson PE. Crack growth and development of fracture zones in plain concrete and similar materials. Sweden1981. p. 177.

[15] Rubinstein AA. Macrocrack interaction with semi-infinite microcrack array. International Journal of Fracture. 1985;27:113-9.

[16] Petrova V, Tamuzs V, Romalis N. A Survey of Macro-Microcrack Interaction Problems. Applied Mechanics Reviews. 2000;53:117-46.

[17] Tamuzs V, Romalis N, Petrova V. Influence of microcracks on thermal fracture of macrocrack. Theoretical and Applied Fracture Mechanics. 1993;19:207-25.

[18] Benedetti M, Fontanari V, Monelli BD, Beghini M. A fully parametric weight function for inclined edge cracks with a kink. Engineering Fracture Mechanics. 2015;136:195-212.

[19] Feng X-Q, Li J-Y, Ma L, Yu S-W. Analysis on interaction of numerous microcracks. Computational Materials Science. 2003;28:454-61.

[20] Zhou X, Wang Y, Qian Q. Numerical simulation of crack curving and branching in brittle materials under dynamic loads using the extended non-ordinary state-based peridynamics. European Journal of Mechanics - A/Solids. 2016;60:277-99.

[21] Wang H, Liu Z, Xu D, Zeng Q, Zhuang Z. Extended finite element method analysis for shielding and amplification effect of a main crack interacted with a group of nearby parallel microcracks. International Journal of Damage Mechanics. 2016;25:4-25.

[22] Budyn É, Zi G, Moës N, Belytschko T. A method for multiple crack growth in brittle materials without remeshing. International Journal for Numerical Methods in Engineering. 2004;61:1741-70.

[23] Moës N, Dolbow J, Belytschko T. A finite element method for crack growth without remeshing. International Journal for Numerical Methods in Engineering. 1999;46:131-50.

[24] Zhuang Z, Cheng B-B. Development of X-FEM methodology and study on mixed-mode crack propagation. Acta Mechanica Sinica. 2011;27:406-15.

[25] Zhuang Z, Cheng BB. Equilibrium state of mode-I sub-interfacial crack growth in bi-materials. International Journal of Fracture. 2011;170:27-36.

[26] Zhuang Z, Cheng B. A novel enriched CB shell element method for simulating arbitrary crack growth in pipes. Science China Physics, Mechanics and Astronomy. 2011;54:1520-31.

[27] Bobaru F, Zhang G. Why do cracks branch? A peridynamic investigation of dynamic brittle fracture. International Journal of Fracture. 2015;196:59-98.

[28] Silling SA, Askari E. A meshfree method based on the peridynamic model of solid mechanics. Computers and Structures. 2005;83:1526-35.

[29] Silling SA. Reformulation of elasticity theory for discontinuities and long-range forces. Journal of the Mechanics and Physics of Solids. 2000;48:175-209.

[30] Silling SA, Weckner O, Askari E, Bobaru F. Crack nucleation in a peridynamic solid. International Journal of Fracture. 2010;162:219-27.

[31] Huang D, Lu G, Qiao P. An improved peridynamic approach for quasi-static elastic deformation and brittle fracture analysis. International Journal of Mechanical Sciences. 2015;94-95:111-22.

[32] Ha YD, Bobaru F. Characteristics of dynamic brittle fracture captured with peridynamics. Engineering Fracture Mechanics. 2011;78:1156-68.

[33] Bobaru F, Hu W. The Meaning, Selection, and Use of the Peridynamic Horizon and its Relation to Crack Branching in Brittle Materials. International Journal of Fracture. 2012;176:215-22.

[34] Basoglu MF, Zerin Z, Kefal A, Oterkus E. A computational model of peridynamic theory for deflecting behavior of crack propagation with micro-cracks. Computational Materials Science. 2019;162:33-46.

[35] Vazic B, Wang H, Diyaroglu C, Oterkus S, Oterkus E. Dynamic propagation of a macrocrack interacting with parallel small cracks. AIMS Materials Science. 2017;4:118-36.

[36] Silling SA, Epton M, Weckner O, Xu J, Askari E. Peridynamic states and constitutive modeling. Journal of Elasticity. 2007;88:151-84.

[37] Silling SA, Lehoucq RB. Convergence of Peridynamics to Classical Elasticity Theory. Journal of Elasticity. 2008;93:13.

[38] Oterkus E, Madenci E. Peridynamic Analysis of Fiber-Reinforced Composite Materials. Journal of Mechanics of Materials and Structures. 2012;7:45-84.

[39] Shang S, Qin X, Li H, Cao X. An application of non-ordinary state-based peridynamics theory in cutting process modelling of unidirectional carbon fiber reinforced polymer material. Composite Structures. 2019;226:111194.

[40] AlKhateab B, Tabrizi IE, Zanjani JSM, Rahimi MN, Poudeh LH, Kefal A, et al. Damage mechanisms in CFRP/HNT laminates under flexural and in-plane shear loadings using experimental and numerical methods. Composites Part A: Applied Science and Manufacturing. 2020;136:105962.

[41] Ghajari M, Iannucci L, Curtis P. A peridynamic material model for the analysis of dynamic crack propagation in orthotropic media. Computer Methods in Applied Mechanics and Engineering. 2014;276:431-52.

[42] Ozdemir M, Kefal A, Imachi M, Tanaka S, Oterkus E. Dynamic fracture analysis of functionally graded materials using ordinary state-based peridynamics. Composite Structures. 2020;244:112296.

[43] Rahimi MN, Kefal A, Yildiz M. An improved ordinary-state based peridynamic formulation for modeling FGMs with sharp interface transitions. International Journal of Mechanical Sciences. 2021;197:106322.

[44] Oterkus E, Madenci E, Weckner O, Silling S, Bogert P, Tessler A. Combined finite element and peridynamic analyses for predicting failure in a stiffened composite curved panel with a central slot. Composite Structures. 2012;94:839-50.

[45] Kilic B, Madenci E. Coupling of Peridynamic Theory and the Finite Element Method. Journal of Mechanics of Materials and Structures. 2010;5:707-33.

[46] De Meo D, Diyaroglu C, Zhu N, Oterkus E, Siddiq MA. Modelling of stress-corrosion cracking by using peridynamics. International Journal of Hydrogen Energy. 2016;41:6593-609.

[47] Askari E, Bobaru F, Lehoucq RB, Parks ML, Silling SA, Weckner O. Peridynamics for multiscale materials modeling. Journal of Physics: Conference Series. 2008;125:012078.

[48] Oterkus S, Madenci E, Agwai A. Peridynamic thermal diffusion. Journal of Computational Physics. 2014;265:71-96.

[49] Oterkus S, Madenci E, Agwai A. Fully coupled peridynamic thermomechanics. Journal of the Mechanics and Physics of Solids. 2014;64:1-23.

[50] Madenci E, Oterkus S. Ordinary state-based peridynamics for plastic deformation according to von Mises yield criteria with isotropic hardening. Journal of the Mechanics and Physics of Solids. 2016;86:192-219.

[51] Madenci E, Oterkus E. Peridynamic Theory and Its Applications. New York: Springer, 2014.

[52] Javili A, Morasata R, Oterkus E, Oterkus S. Peridynamics review. Mathematics and Mechanics of Solids. 2019;24:3714-39.

[53] Kefal A, Sohouli A, Oterkus E, Yildiz M, Suleman A. Topology optimization of cracked structures using peridynamics. Continuum Mechanics and Thermodynamics. 2019;31:1645-72.

[54] Habibian A, Sohouli A, Kefal A, Nadler B, Yildiz M, Suleman A. Multi-material topology optimization of structures with discontinuities using Peridynamics. Composite Structures. 2021;258:113345.

[55] Sohouli A, Kefal A, Abdelhamid A, Yildiz M, Suleman A. Continuous density-based topology optimization of cracked structures using peridynamics. Structural and Multidisciplinary Optimization. 2020;62:2375-89.

[56] Rahimi MN, Kefal A, Yildiz M, Oterkus E. An ordinary state-based peridynamic model for toughness enhancement of brittle materials through drilling stop-holes. International Journal of Mechanical Sciences. 2020;182:105773.

[57] Karpenko O, Oterkus S, Oterkus E. Influence of Different Types of Small-Size Defects on Propagation of Macro-cracks in Brittle Materials. Journal of Peridynamics and Nonlocal Modeling. 2020;2:289-316.

[58] Kilic B. Peridynamic Theory for Progressive Failure Prediction in Homogeneous and Heterogeneous Materials: The University of Arizona., 2008.